

# Semiclassical propagation of Wigner functions

T. Dittrich<sup>1,2</sup>, E. A. Gómez<sup>1,2</sup>, L. A. Pachón<sup>1,2</sup>

<sup>1</sup>*Departamento de Física, Universidad Nacional de Colombia, Bogotá D.C., Colombia.*

<sup>2</sup>*CeiBA – Complejidad, Bogotá D.C., Colombia.*

(Dated: June 29, 2021)

## Abstract

We present a comprehensive study of semiclassical phase-space propagation in the Wigner representation, emphasizing numerical applications, in particular as an initial-value representation. Two semiclassical approximation schemes are discussed: The propagator of the Wigner function based on van Vleck's approximation replaces the Liouville propagator by a quantum spot with an oscillatory pattern reflecting the interference between pairs of classical trajectories. Employing phase-space path integration instead, caustics in the quantum spot are resolved in terms of Airy functions. We apply both to two benchmark models of nonlinear molecular potentials, the Morse oscillator and the quartic double well, to test them in standard tasks such as computing auto-correlation functions and propagating coherent states. The performance of semiclassical Wigner propagation is very good even in the presence of marked quantum effects, e.g., in coherent tunneling and in propagating Schrödinger cat states, and of classical chaos in four-dimensional phase space. We suggest options for an effective numerical implementation of our method and for integrating it in Monte-Carlo–Metropolis algorithms suitable for high-dimensional systems.

PACS numbers: 03.65.Sq, 31.15.Gy, 31.15.Kb

## I. INTRODUCTION

Molecular dynamics, by the spatial and temporal scales it involves, straddles the borderline between quantum and classical behavior. Quantum effects—above all the very concept of chemical reaction—are obviously crucial. Notwithstanding, a good deal of a molecule’s external and even internal motion can be understood on purely classical grounds: precisely the situation for which semiclassical methods have been conceived and are optimally suited. Moreover, recent developments in chemical physics, experimental as well as theoretical, are advancing vigorously in the direction of complex time evolution and high excitations. This faces adiabatic techniques like even time-dependent density-functional theory (TDDFT) [1] and time-dependent Hartree [2, 3] with formidable challenges while it favors semiclassical approaches which do not suffer from limitations in this respect.

Therefore, the modest renaissance semiclassics in the time domain (for a comprehensive review see [4]) is presently enjoying comes as no surprise. It includes approaches in configuration space as well as less established phase-space methods. The well-known shortcomings plaguing semiclassics in coordinate representation (based on WKB approximations [5] and the van-Vleck–Gutzwiller propagator [6–8]), such as divergences at caustics and the root-search problem, have largely been overcome by sophisticated refinements of the original method [9]. Remarkably, most of them already switch internally to mixed representations (combining position with momentum) or full phase space in order to smooth out divergences and to reduce the set of contributing classical solutions to the neighbourhood of a single trajectory, permitting the construction of initial-value representations (IVRs): uniform approximations [10–12], semiclassical IVRs [9, 13–15] (for reviews see [16–18]), Gaussian-wavepacket propagation [19] with its numerous ramifications, notably the Herman-Kluk propagator [20–22] and Heller’s cellular dynamics [23]. A similar but independent approach, the dephasing representation [24–26] employs the shadowing lemma for chaotic dynamics to represent the classical flow through a Planck cell by a single trajectory in a semiclassical approximation for correlation functions.

These methods have gained widespread acceptance in practical applications but tend to be technically cumbersome. Their implementation in *ab initio* molecular-dynamics simulation with “on the fly” update of the electronic evolution [27, 28] has been proposed [29]. It has to cope, though, with the high computational costs of calculating Hessians for the potential-

energy surface of the electron sector—so much so that recourse is sought even at a complete suppression of determinantal prefactors [30].

Semiclassical approximations working directly in phase space promise a fresh, structurally more transparent approach. They are inherently free of the above problems and thus offer a number of tempting advantages: (i) phase-space propagation provides a natural exact IVR by construction, without Gaussian smoothing, (ii) it can be formulated exclusively in terms of canonically invariant quantities (no projection required) that (iii) allow for simple geometrical interpretations, (iv) as far as determinantal prefactors arise, they are also canonically invariant, and (v) being based on the density operator, not on wavefunctions, the extension to non-unitary time evolution is immediate, opening access to decoherence and dissipation [31].

Yet there is a price to be paid. The two representations mainly considered as candidates for semiclassical phase-space propagation both come with their specific virtues and vices: The Husimi function [32] is based on coherent states [33], hence closely related to semiclassical IVRs and Gaussian-wavepacket propagation. Coherent states possess a natural interpretation in terms of classical probabilities but are overcomplete, contain arbitrary parameters, and, in order to work optimally, require to complexify phase space [22, 34]. The Wigner function [35–37], by contrast, provides a parameter-free one-to-one representation of the full density operator but encodes information on quantum coherences as small-scale (“sub-Planckian”) oscillatory fringes [38, 39]. They prevent a probability interpretation and pose serious problems for their propagation, pointed out more than 30 years ago by Heller [40].

Owing to these seemingly prohibitive difficulties, the semiclassical propagation of Wigner functions still awaits being explored in its full potentiality. For a long time, it has been almost synonymous to a mere classical propagation of phase-space distributions, discarding quantum effects in the time evolution altogether [41, 42]. As a first attempt to improve on this so-called classical Wigner model, it suggests itself to include higher-order terms in  $\hbar$  in the quantum analogue of the Poisson bracket, the Moyal bracket [38], upon integrating the evolution equation for the Wigner function. Such additive quantum corrections give rise to accordingly modified “quantum trajectories” [43–47]. However, they tend to become unstable even for short propagation time [48] and suffer from other practical and fundamental problems [49]: As we shall point out below, the very concept of propagating along single

deterministic trajectories is inadequate even in the semiclassical regime.

A more convincing alternative has emerged in the context of quantum chaos where semiclassical Wigner functions [38, 50, 51] are appreciated as valuable tools, e.g., in the study of scars in wavefunctions and of spectral features related to them [52–54]. By applying semiclassical approximations directly to the finite-time propagator, expanding the phase instead of the underlying evolution equation, an appropriate phase-space propagation method for semiclassical Wigner functions has been achieved [55]. It features, in a geometrically appealing manner, *pairs* of (real) classical trajectories and the symplectic area enclosed between them as their classical underpinning—not surprisingly in view of the well-known pairing of paths and diagrams, one forward, one backward in time, as it occurs in the propagation of quantities bilinear in the state vector, particularly the density operator.

While this technique is tailor-made to time-evolve the specific class of semiclassical Wigner functions [38, 50, 51, 54], semiclassical approximations to the propagator proper, independent of the nature of initial and final states, have been constructed [56] on basis of phase-space path integrals [57] and of the Weyl-transformed van Vleck propagator [52]. This approach opens the door towards a far broader range of applications. It has already proven fruitful in an analysis of the spectral form factor of classically chaotic systems in terms of phase-space manifolds [58].

Here, by difference, we pretend to demonstrate its viability as a practical instrument for the propagation of molecular systems, including in particular numerical simulations. We therefore focus on its performance in benchmark models established in chemical physics like the Morse oscillator and the quartic double well and study standard tasks such as propagating Gaussians and computing autocorrelation functions. We are confident that the remarkable accuracy and robustness of the scheme and its unexpected numerical stability and efficiency suggest it as a new competitive option in semiclassical propagation.

In Sec. II, we introduce the basic building blocks of our method, specify our two main approaches, via the van-Vleck propagator and via phase-space path integration, and discuss general properties of the semiclassical Wigner propagator, such as its geometrical structure and its asymptotics towards the classical limit and towards weak anharmonicity. This section partially corresponds to a more detailed account of material already published in Ref. [56]. Readers mainly interested in numerical results might proceed directly to Sec. III, dedicated to a broad survey of the performance of semiclassical Wigner propagation for prototypical

models of nonlinear molecular potentials, in the computation of dynamical functions like autocorrelations as well as of detailed structures in phase space. We also test our method in particularly challenging situations, involving strong quantum effects, such as the reproduction of coherent tunneling and the propagation of Schrödinger-cat states, or a classically chaotic dynamics. Strategies to optimize the implementation of this method in numerical, including Monte-Carlo-like, algorithms are suggested in Sec. IV. We conclude in Sec. V with an outlook to immediate extensions of our work.

## II. CONSTRUCTING THE SEMICLASSICAL WIGNER PROPAGATOR

### A. Definitions and basic relations

Alternative to its definition as a Weyl-ordered transform of the density operator [36], the Wigner function can be introduced as the expectation value of phase-space reflection operators [51] or as expansion coefficient function in a basis of phase-space displacement operators [59], besides other options. For our purposes, the standard definition suffices,

$$W(\mathbf{r}) = \frac{1}{2\pi\hbar} \int d^f q' e^{-i\mathbf{p}\cdot\mathbf{q}'/\hbar} \left\langle \mathbf{q} + \frac{\mathbf{q}'}{2} \left| \hat{\rho} \right| \mathbf{q} - \frac{\mathbf{q}'}{2} \right\rangle, \quad (1)$$

where  $\hat{\rho}$  denotes the density operator and  $\mathbf{r} = (\mathbf{p}, \mathbf{q})$  is a vector in  $2f$ -dimensional phase space (we adopt this ordering throughout the paper but assign  $q$  to the horizontal and  $p$  to the vertical axis in phase-space plots).

We shall restrict ourselves to unitary time evolution within the dynamical group  $\hat{U}(t) = \exp(-i\hat{H}t/\hbar)$  generated by a time-independent Hamiltonian  $\hat{H}$ . The extension to time-dependent Hamiltonians is immediate but will be suppressed to avoid technicalities. The von-Neumann equation for the density operator,  $d\hat{\rho}/dt = (-i/\hbar)[\hat{H}, \hat{\rho}]$ , translates into an equation of motion for the Wigner function,  $(\partial/\partial t)W(\mathbf{r}, t) = \{H_W(\mathbf{r}), W(\mathbf{r}, t)\}_{\text{Moyal}}$ , involving the Weyl symbol  $H_W(\mathbf{r})$  of the Hamiltonian  $\hat{H}$ . For  $\hbar \rightarrow 0$ , the Moyal bracket  $\{\cdot, \cdot\}_{\text{Moyal}}$  [36, 37] converges to the Poisson bracket.

The time evolution of the Wigner function over a finite time can be expressed as an integral kernel, the Wigner propagator  $G_W(\mathbf{r}'', \mathbf{r}', t)$ ,

$$W(\mathbf{r}'', t) = \int d^{2f} r' G_W(\mathbf{r}'', \mathbf{r}', t) W(\mathbf{r}', 0). \quad (2)$$

It forms a one-parameter group, implying in particular the initial condition  $G_W(\mathbf{r}'', \mathbf{r}', 0) = \delta(\mathbf{r}'' - \mathbf{r}')$  and the composition law

$$G_W(\mathbf{r}'', \mathbf{r}', t) = \int d^{2f} r G_W(\mathbf{r}'', \mathbf{r}, t - t') G_W(\mathbf{r}, \mathbf{r}', t'). \quad (3)$$

An important quantity that must not be confused with the Wigner propagator is the Weyl transform of the evolution operator  $\hat{U}(t)$ , referred to as the Weyl propagator for short [51],

$$U_W(\mathbf{r}, t) = \int d^f q' e^{\frac{i}{\hbar} \mathbf{p} \cdot \mathbf{q}'} \left\langle \mathbf{q} + \frac{\mathbf{q}'}{2} \left| \hat{U}(t) \right| \mathbf{q} - \frac{\mathbf{q}'}{2} \right\rangle. \quad (4)$$

It cannot be used to propagate Wigner functions as it stands, but is related to the Wigner propagator by a self-convolution [55–57],

$$G_W(\mathbf{r}'', \mathbf{r}', t) = \frac{1}{(2\pi\hbar)^{2f}} \int d^{2f} R e^{\frac{i}{\hbar}(\mathbf{r}'' - \mathbf{r}') \wedge \mathbf{R}} U_W^*(\tilde{\mathbf{r}}_-, t) U_W(\tilde{\mathbf{r}}_+, t), \quad (5)$$

with  $\tilde{\mathbf{r}}_{\pm} \equiv (\mathbf{r}' + \mathbf{r}'' \pm \mathbf{R})/2$ . It serves as a starting point for the construction of semiclassical approximations, based on the van-Vleck propagator (Sec. II B) as well as on phase-space path integration (Sec. II C).

## B. van Vleck approximation for the Wigner propagator

A straightforward route towards a semiclassical Wigner propagator is replacing the Weyl propagator in Eq. (5) by the Weyl transform of the van Vleck propagator [51, 52, 57]. Transformed from the energy to the time domain, it reads [51, 57],

$$U_W(\mathbf{r}, t) = 2^f \sum_j \frac{\exp\left(\frac{i}{\hbar} S_j(\mathbf{r}, t) - i\mu_j \frac{\pi}{2}\right)}{\sqrt{|\det(\mathbf{M}_j(\mathbf{r}, t) + \mathbf{I})|}}. \quad (6)$$

The sum runs over all classical trajectories  $j$  connecting phase-space points  $\mathbf{r}'_j$  to  $\mathbf{r}''_j$  in time  $t$  such that  $\mathbf{r} = \tilde{\mathbf{r}}_j \equiv (\mathbf{r}'_j + \mathbf{r}''_j)/2$  (midpoint rule).  $\mathbf{M}_j$  and  $\mu_j$  are its stability matrix and Maslov index, respectively. The action  $S_j(\mathbf{r}_j, t) = A_j(\mathbf{r}_j, t) - H_j(\mathbf{r}, t) t$ , with  $H_j(\mathbf{r}, t) \equiv H_W(\mathbf{r}_j, t)$ , the Weyl Hamiltonian evaluated on the trajectory  $j$  (to be distinguished from  $H_W(\mathbf{r}, t)$ ) and  $A_j$ , the symplectic area enclosed between the trajectory and the straight line (chord) connecting  $\mathbf{r}'_j$  to  $\mathbf{r}''_j$  [52] (chord rule, vertically hashed areas  $A_{j\pm}$  in Fig. 1).

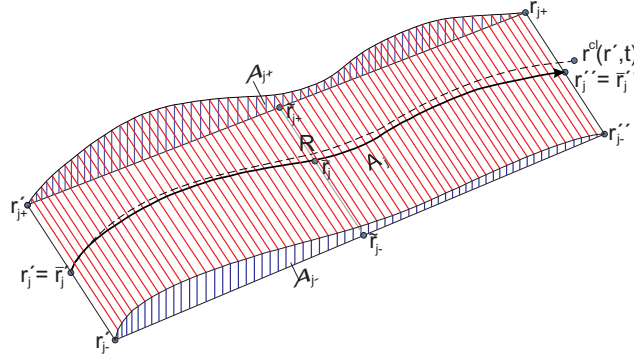


FIG. 1: Symplectic areas entering the van-Vleck-based semiclassical Wigner propagator, Eqs. (10, 11). The vertically hashed areas correspond to the phases  $A_{j\pm}$  of the Weyl propagators (6) according to the chord rule. The symplectic area (slanted hatching) enclosed between the two classical trajectories  $\mathbf{r}_{j\pm}(t)$  and the two transverse vectors  $\mathbf{r}'_{j+} - \mathbf{r}'_{j-}$  and  $\mathbf{r}''_{j+} - \mathbf{r}''_{j-}$  determines the phase (11) of the propagator. The classical trajectory  $\mathbf{r}^{cl}(\mathbf{r}', t)$  (dashed) is to be distinguished from the propagation path  $\bar{\mathbf{r}}_j(\mathbf{r}', t)$  (bold) connecting the initial argument  $\mathbf{r}'$  of the propagator to the final one,  $\mathbf{r}''$ .

Substituting Eq. (6) in (5), one arrives at

$$G_W(\mathbf{r}'', \mathbf{r}', t) = \frac{1}{(\pi\hbar)^{2f}} \sum_{j_-, j_+} \int d^{2f} R e^{\frac{-i}{\hbar}(\mathbf{r}'' - \mathbf{r}') \wedge \mathbf{R}} \frac{\exp\left[\frac{i}{\hbar}\left(S_{j_+}(\tilde{\mathbf{r}}_{j_+}, t) - S_{j_-}(\tilde{\mathbf{r}}_{j_-}, t)\right) - i(\mu_{j_+} - \mu_{j_-})\frac{\pi}{2}\right]}{|\det[\mathbf{M}_{j_-}(\mathbf{r}, t) + \mathbb{1}] \det[\mathbf{M}_{j_+}(\mathbf{r}, t) + \mathbb{1}]|^{1/2}}, \quad (7)$$

where indices  $j_{\pm}$  refer to classical trajectories contributing to the Weyl propagators  $U_W(\tilde{\mathbf{r}}_{\pm}, t)$  in Eq. (5). The principal challenge is now evaluating the  $R$ -integration. As it stands, Eq. (7) couples the two classical trajectories  $\mathbf{r}_{j_-}$ ,  $\mathbf{r}_{j_+}$ , to one another only indirectly via  $\mathbf{R}$ , the separation of their respective midpoints. This changes as soon as an integration by stationary-phase approximation is attempted, consistent with the use of the van Vleck propagator. Stationary points are specified implicitly by the condition  $\mathbf{r}'' - \mathbf{r}' = (\mathbf{r}''_{j_-} - \mathbf{r}'_{j_-} + \mathbf{r}''_{j_+} - \mathbf{r}'_{j_+})/2$ . Combined with the midpoint rule  $\mathbf{r}' + \mathbf{r}'' \pm \mathbf{R} = \mathbf{r}'_{j_{\pm}} + \mathbf{r}''_{j_{\pm}}$ , this implies

$$\mathbf{r}' = \bar{\mathbf{r}}'_j \equiv (\mathbf{r}'_{j_-} + \mathbf{r}'_{j_+})/2, \quad \mathbf{r}'' = \bar{\mathbf{r}}''_j \equiv (\mathbf{r}''_{j_-} + \mathbf{r}''_{j_+})/2. \quad (8)$$

Equation (8) constitutes a simple geometrical rule for semiclassical Wigner propagation [51]: It is based on pairs of classical trajectories  $j_+$ ,  $j_-$ , that need not coincide with one another nor with the trajectories passing through  $\mathbf{r}'$  and  $\mathbf{r}''$  but must have  $\mathbf{r}'$  midway between

their respective initial points  $\mathbf{r}'_{j_{\pm}}$  and likewise for  $\mathbf{r}''$ . This condition is trivially fulfilled for identical pairs  $\mathbf{r}_{j_-}(t) = \mathbf{r}_{j_+}(t)$ , as a type of diagonal approximation. By including also non-diagonal terms, i.e., non-identical trajectory pairs, we add classical information contained in third-order terms in the action and partially compensate for the general limitations of the van Vleck approach on the level of wavepackets. This becomes particularly evident in the case of pure initial states  $\rho' = |\psi'\rangle\langle\psi'|$ : Applying the van Vleck propagator in position representation separately to ket and bra, allowing for off-diagonal terms in the ensuing double sum over classical orbits, and then transforming back to the final Wigner function leads to the same result as the present derivation, albeit through a more tedious and less transparent route.

To complete the Fresnel integral over  $R$ , we note that

$$\frac{\partial^2}{\partial \mathbf{R}^2} [S_{j_+}(\tilde{\mathbf{r}}_+, t) - S_{j_-}(\tilde{\mathbf{r}}_-, t)] = \frac{\mathbf{J}}{2} \left( \frac{\mathbf{M}_{j_-} - \mathbf{I}}{\mathbf{M}_{j_-} + \mathbf{I}} - \frac{\mathbf{M}_{j_+} - \mathbf{I}}{\mathbf{M}_{j_+} + \mathbf{I}} \right) = \frac{\mathbf{J}(\mathbf{M}_{j_-} - \mathbf{M}_{j_+})}{(\mathbf{M}_{j_-} + \mathbf{I})(\mathbf{M}_{j_+} + \mathbf{I})}, \quad (9)$$

where  $\mathbf{J}$  denotes the  $2f \times 2f$  symplectic unit matrix [52]. Combined with the determinantal prefactors inherited from the van Vleck propagator, this produces

$$G_{\text{W}}^{\text{vV}}(\mathbf{r}'', \mathbf{r}', t) = \frac{4^f}{h^f} \sum_j \frac{2 \cos\left(\frac{1}{\hbar} S_j^{\text{vV}}(\mathbf{r}'', \mathbf{r}', t) - f \frac{\pi}{2}\right)}{|\det(\mathbf{M}_{j_+} - \mathbf{M}_{j_-})|^{1/2}}, \quad (10)$$

our main result for the semiclassical Wigner propagator in van Vleck approximation. The phase is determined by

$$\begin{aligned} S_j^{\text{vV}}(\mathbf{r}'', \mathbf{r}', t) &= (\tilde{\mathbf{r}}_{j_+} - \tilde{\mathbf{r}}_{j_-}) \wedge (\mathbf{r}'' - \mathbf{r}') + S_{j_+} - S_{j_-} \\ &= \int_0^t ds [\dot{\bar{\mathbf{r}}}_j(s) \wedge \mathbf{R}_j(s) - H_{j_+}(\mathbf{r}_{j_+}) + H_{j_-}(\mathbf{r}_{j_-})], \end{aligned} \quad (11)$$

with  $\bar{\mathbf{r}}_j(s) \equiv (\mathbf{r}_{j_-}(s) + \mathbf{r}_{j_+}(s))/2$  and  $\mathbf{R}_j(s) \equiv \mathbf{r}_{j_+}(s) - \mathbf{r}_{j_-}(s)$ . Besides the two Hamiltonian terms it includes the symplectic area enclosed between the two trajectory sections and the vectors  $\mathbf{r}'_{j_+} - \mathbf{r}'_{j_-}$  and  $\mathbf{r}''_{j_+} - \mathbf{r}''_{j_-}$  (Fig. 1).

In the following we list a number of general features of Eqs. (10,11):

- i. Equation (10) replaces the Liouville propagator,

$$G_{\text{W}}^{\text{cl}}(\mathbf{r}'', \mathbf{r}', t) = \delta[\mathbf{r}'' - \mathbf{r}^{\text{cl}}(\mathbf{r}', t)], \quad (12)$$

localized on the classical trajectory  $\mathbf{r}^{\text{cl}}(\mathbf{r}', t)$  initiated in  $\mathbf{r}'$ , by a ‘‘quantum spot’’, a smooth distribution peaked at the support of the classical propagator but spreading



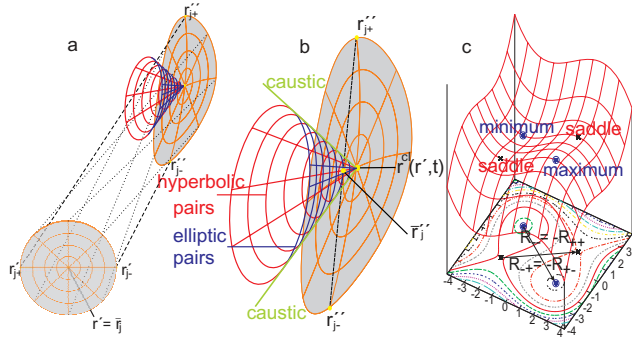


FIG. 2: Classical skeleton of the semiclassical Wigner propagator according to Eqs. (10,11). A set of initial points  $\mathbf{r}'_{j\pm}$  (panel a, left target pattern) surrounding the initial point  $\mathbf{r}'$  of the propagation path is propagated along classical trajectories (dotted lines), giving rise to a corresponding set of final points  $\mathbf{r}''_{j\pm}$  (right deformed target pattern). The manifold formed by their midpoints (cone-like structure, panel b) constitutes the “illuminated area”, the support of the semiclassical propagator. Inside this area, two trajectory pairs contribute to each point, one of them elliptic (“upper” shell of the cone, blue), the other hyperbolic (“lower” shell, red). Its boundary gives rise to caustics in phase space where the two trajectory pairs collapse into one. Panel c depicts the generic structure of the underlying phase as a function of the integration variable  $\mathbf{R}$  in Eq. (7), an odd cubic polynomial of the phase-space coordinates with two extrema, a minimum and a maximum (blue  $\odot$  symbols) and two saddles (red  $\times$  symbols), corresponding to the elliptic and the hyperbolic trajectory pairs, respectively.

into the adjacent phase space and structured by an oscillatory pattern that results from the interference of the trajectories involved.

- ii. The propagator (10) does involve determinantal prefactors. However, they do not result from any projection onto a subspace like  $\mathbf{q}$  or  $\mathbf{p}$  and are invariant [52] under linear canonical (affine) transformations [60].
- iii. It deviates from the Liouville propagator only if the potential is anharmonic. For a purely harmonic potential, the two operations, propagation in time and forming midpoints between trajectories, commute, so that all midpoint paths  $\bar{\mathbf{r}}_j(t) = [\mathbf{r}_{j-}(t) + \mathbf{r}_{j+}(t)]/2$  coincide with each other and with the classical trajectory  $\mathbf{r}^{\text{cl}}(\mathbf{r}', t)$ . This singularity restores the classical delta function on  $\mathbf{r}^{\text{cl}}(\mathbf{r}', t)$ , see Sec. IID 3.

- iv. By contrast to position-space semiclassics [8], the number of trajectory pairs contributing to the summation in Eq. (10) ranges between 0, 1, and 2 following a universal pattern (Fig. 2): Within an “illuminated area”, a sector with its tip on the classical trajectory, the sum contains two trajectory pairs (four stationary points, Fig. 2c). In the “shadow region” outside this sector, stationarity cannot be fulfilled by real trajectories. Along the border there is exactly one solution (two stationary points). Unexpected in phase space, this caustic arises as the projection onto phase space of the manifold of midpoints  $\bar{\mathbf{r}}_j'' = (\mathbf{r}_{j-}'' + \mathbf{r}_{j+}'')/2$  (Fig. 2b).
- v. The set of trajectory pairs to enter the calculation of the propagator is only restricted by the midpoint rule (8). However, this does not constitute a double-sided boundary condition since every pair fulfilling Eq. (8) for the initial points contributes a valid data point to the propagator: *no root-search*. The freedom in the choice of trajectory pairs can be exploited to optimize algorithms, see Sec. IV A 3.
- vi. Of the two trajectory pairs contributing to the illuminated area, exactly one is elliptic, associated to a pair of opposite extrema of the action, one is hyperbolic and associated to a pair of saddles (Fig. 2c). They can be distinguished by monitoring  $\text{sgn det}(\mathbf{M}_{j+} - \mathbf{M}_{j-})$ , positive for the former and negative for the latter. The two sets form separate sheets of the action (11). Within each of them, amplitude and phase of the propagator are slowly varying functions of  $\mathbf{r}''$ , facilitating their numerical treatment, see Sec. IV.
- vii. The propagator’s oscillatory pattern encodes information on quantum coherences and allows us to propagate the “sub-Planckian oscillations” that characterize the Wigner function, solving the problem of the “dangerous cross terms” pointed out by Heller [40]. See Sec. III E.
- viii. The principle of propagation by trajectory pairs is consistent with the properties of a dynamical group. It translates the concatenation of propagators into a continuation of trajectories, if the convolution (3) is evaluated by stationary phase as well.
- ix. Equations (10, 11) fail if the stationary points approach each other too closely. This is the case near the central peak of the propagator on the classical trajectory and along the caustics mentioned above. The same problem arises in the limits  $t \rightarrow 0$ ,  $\hbar \rightarrow 0$ ,

and of weak anharmonicity. It can be overcome by means of a uniform approximation to the  $R$ -integration in Eq. (7), see Sec. IID 2.

- x. As a consequence of the underlying van Vleck approximation, the propagator (10) is not properly normalized. Specifically, the slow decay of its oscillatory tail renders it nonintegrable with respect to its initial or final arguments, see Sec. III C 1 for quantitative details. The problem is solved by the same uniform approximation as announced above.

### C. Path-integral approach

The quality of the van Vleck approximation (10) to the Wigner propagator is limited by its principal ingredient, the van Vleck propagator itself. Just as in configuration-space propagation, a comprehensive solution is provided on the basis of path integrals [61, 62]. In phase space an analogous theoretical framework is available since the seminal work of Marinov [57], largely following Feynman: Time is discretized into  $N$  equidistant sections  $t_n = t' + n\Delta t$ , where  $\Delta t = T/N$  and  $T = t'' - t'$  is the time span to be propagated over. At each  $t_n$ , two short-time propagators, composed of the corresponding Weyl propagators according to Eq. (5), are concatenated by means of Eq. (3). In the continuous limit  $N \rightarrow \infty$ ,  $\Delta t \rightarrow 0$ , the full propagator is obtained as a double path integral comprising two distinct path variables  $\mathbf{r}$  and  $\mathbf{R}$ , inherited, respectively, from Eqs. (3) and (5),

$$G_{\text{W}}(\mathbf{r}'', t''; \mathbf{r}', t') = h^{-f} \int \text{D}r \int \text{D}R e^{\frac{i}{\hbar} S(\{\mathbf{r}\}, \{\mathbf{R}\})} \quad (13)$$

with an action integral

$$S(\{\mathbf{r}\}, \{\mathbf{R}\}) = \int_{t'}^{t''} \text{d}s \left\{ \dot{\mathbf{r}}(s) \wedge \mathbf{R}(s) + H_{\text{W}} \left[ \mathbf{r}(s) + \frac{1}{2} \mathbf{R}(s) \right] - H_{\text{W}} \left[ \mathbf{r}(s) - \frac{1}{2} \mathbf{R}(s) \right] \right\}. \quad (14)$$

Only  $\mathbf{r}(t)$  is subject to boundary conditions  $\mathbf{r}(t') = \mathbf{r}'$  and  $\mathbf{r}(t'') = \mathbf{r}''$  while  $\mathbf{R}(t)$  is free and may be associated to quantum fluctuations.

For this subsection, we restrict ourselves to a single degree of freedom,  $\mathbf{r} = (p, q)$ , and to standard Hamiltonians  $H(\hat{p}, \hat{q}, t) = T(\hat{p}) + V(\hat{q}, t)$ ,  $T(\hat{p}) = \hat{p}^2/2m$ , but admit an explicit time dependence and an arbitrary degree of nonlinearity of the potential. In this case, the Weyl Hamiltonian,  $H_{\text{W}}(p, q)$ , is obtained by replacing the operators  $\hat{p}$ ,  $\hat{q}$  in  $H$  with corresponding real variables,  $H_{\text{W}}(p, q) = T(p) + V(q, t)$ .

Returning to discrete time, we are faced with evaluating the action

$$S_N(\{\mathbf{r}\}, \{\mathbf{R}\}) = \sum_{n=1}^N \left\{ \Delta \mathbf{r}_n \wedge \mathbf{R}_n + \left[ H_W \left( \bar{\mathbf{r}}_n + \frac{1}{2} \mathbf{R}_n \right) - H_W \left( \bar{\mathbf{r}}_n - \frac{1}{2} \mathbf{R}_n \right) \right] \Delta t \right\}, \quad (15)$$

denoting  $\Delta \mathbf{r}_n \equiv \mathbf{r}_n - \mathbf{r}_{n-1}$  and  $\bar{\mathbf{r}}_n \equiv (\mathbf{r}_{n-1} + \mathbf{r}_n)/2$ . To obtain a semiclassical approximation, we expand the action (15) in  $\mathbf{r}_n$  around a classical trajectory  $\mathbf{r}_n^{\text{cl}}$  defined implicitly in discrete time by  $\Delta p_n^{\text{cl}} = -V'(\bar{q}_n^{\text{cl}}, t_n) \Delta t$ ,  $\Delta q_n^{\text{cl}} = (\bar{p}_n^{\text{cl}}/m) \Delta t$ , and around  $\mathbf{R}_n \equiv 0$ ,  $n = 1, \dots, N$ . By expanding around a single trajectory, we are sampling less classical information than in the van Vleck approximation based on trajectory pairs. This renders our path-integral approach inferior in some respects detailed below. Note that the action (15) is not only an odd polynomial in  $\mathbf{R}_n$ , it is even lacking a linear term, hence  $O(R^3)$ , since according to Hamilton's equations of motion, the first term  $\sim (d\mathbf{r}^{\text{cl}}/dt) \wedge \mathbf{R}(t) = \mathbf{R}(t) \wedge \mathbf{J} \partial H_W(\mathbf{r}^{\text{cl}}) / \partial \mathbf{r}^{\text{cl}}$  cancels exactly the leading order of a Taylor expansion of  $H_W(\mathbf{r}^{\text{cl}} + \mathbf{R}/2) - H_W(\mathbf{r}^{\text{cl}} - \mathbf{R}/2)$  with respect to  $\mathbf{R}$ .

Expanding to third order in all variables (there is no  $O(R^4)$ -term in  $S_N(\{\mathbf{r}\}, \{\mathbf{R}\})$  anyway), this leaves us with

$$S_N(\{\mathbf{r}\}, \{\mathbf{R}\}) = S_N(\{\mathbf{r}^{\text{cl}}\}, \{\mathbf{0}\}) + \sum_{n=1}^N \left[ (\Delta q_n - T''(\bar{p}_n^{\text{cl}}) \bar{p}_n \Delta t) P_n + (\Delta p_n + V''(\bar{q}_n^{\text{cl}}, t_n) \bar{q}_n \Delta t) Q_n + \frac{1}{24} V'''(\bar{q}_n^{\text{cl}}, t_n) Q_n^3 \right]. \quad (16)$$

The  $N$  integrations over the  $R_n$  can now be performed, much like the  $p$ -integrations in the derivation of the Feynman path integral [61, 62], resulting in one-step propagators

$$G_W(\mathbf{r}_n, t_n; \mathbf{r}_{n-1}, t_{n-1}) = \delta [\Delta q_n - T''_n p_{n-1} \Delta t] \nu_n^{-1/3} \text{Ai} \left[ \nu_n^{-1/3} (\Delta p_n + V''_n q_{n-1} \Delta t) \right], \quad (17)$$

where we use shorthands  $T_n = T(\bar{p}_n^{\text{cl}})$  and  $V_n = V(\bar{q}_n^{\text{cl}}, t_n)$  and define  $\nu_n = \hbar^2 V_n''' \Delta t / 8$ . The factor  $\nu_n^{-1/3}$  is analogous to the determinantal prefactors occurring in position-space path integration in that it involves higher derivatives of the potential. Similarly as in the van-Vleck-based Eq. (10), however, it constitutes a mathematically more benign canonical invariant.

Taking into account that the one-step propagators (17) are already written in a frame moving with the classical trajectory, we observe three independent actions of the propagator on the evolving quantum spot: (i), a rigid shift along the classical trajectory, (ii), a rotation (shear) with the linearized phase-space flow around the classical trajectory, if it is elliptic

(hyperbolic), and (iii), quantum Airy-function spreading in the negative  $p$ -direction if  $V'''(q)$  is positive and vice versa. Their concatenation is most conveniently performed in Fourier space, where, under certain conditions fulfilled here [63], the convolution (3) reduces to a mere multiplication. With rescaled coordinates of common dimension  $\sqrt{\text{action}}$ ,

$$\boldsymbol{\rho} = (\eta, \xi) = ((V''/T'')^{-1/4}p, (V''/T'')^{1/4}q), \quad (18)$$

the transformation of the Wigner propagator to Fourier phase space  $\boldsymbol{\gamma} = (\alpha, \beta)$  is given as

$$\tilde{G}_W(\boldsymbol{\gamma}'', t''; \boldsymbol{\gamma}', t') = \frac{1}{4\pi^2} \int d\rho''^2 \int d\rho'^2 e^{-i(\boldsymbol{\gamma}'' \wedge \boldsymbol{\rho}'' - \boldsymbol{\gamma}' \wedge \boldsymbol{\rho}')} G_W(\boldsymbol{\rho}'', t''; \boldsymbol{\rho}', t'). \quad (19)$$

Going to the continuum limit, we thus obtain

$$\tilde{G}_W^{\text{pi}}(\boldsymbol{\gamma}'', t''; \boldsymbol{\gamma}', t') = \delta[\boldsymbol{\gamma}'' - \mathbf{M}(t'', t')\boldsymbol{\gamma}'] \exp \left\{ \frac{-i}{3} \int_{t'}^{t''} dt \sigma(t) [\mathbf{M}(t, t')\boldsymbol{\gamma}']_{\beta} \right\}. \quad (20)$$

Here,  $\mathbf{M}(t, t') = \partial \mathbf{r}^{\text{cl}}(t) / \partial \mathbf{r}^{\text{cl}}(t')$  is the stability matrix of  $\mathbf{r}^{\text{cl}}(t)$ , the subscript  $\beta$  selects the second component of  $\boldsymbol{\gamma}$ , and

$$\sigma(t) \equiv \frac{\hbar^2}{8} \left| \frac{V''[q^{\text{cl}}(t), t]}{T''[p^{\text{cl}}(t)]} \right|^{-3/4} V'''(q^{\text{cl}}(t), t). \quad (21)$$

Inverting the Fourier transform (19) we recover the Wigner propagator. In the following subsection, we work out this result in detail for the specific case  $\sigma(t) \equiv \text{const}$ .

## D. Weak anharmonicity, short-time and classical limits

### 1. Path-integral approach for weak cubic nonlinearity

Equation (20) permits an analytical evaluation in the case of constant second- and third-order derivatives of the potential, which we will discuss in this subsection. It can arise in different scenarios: To begin with, consider a static binding potential with cubic nonlinearity, e.g.,  $V(q) = (m\omega^2/2)q^2(1 + q/3q_{\text{min}})$ , and a trajectory close to the quadratic minimum at  $q_{\text{min}}$ , so that the linearized flow is elliptic. Then  $\partial^3 V(q) / \partial q^3 \equiv V''' = m\omega^2/q_{\text{min}} = \text{const}$  and we can also assume  $(V''/T'')^{1/2} \approx \omega = \text{const}$ . In accordance with Eq. (21), denote  $\sigma = (\hbar^2/8)(m\omega)^{-3/2}V''' = (\hbar^2/8q_{\text{min}})\sqrt{\omega/m}$ . In this case, the stability matrix corresponds to a rotation by  $\tau = \omega(t - t')$ ,

$$\mathbf{M}(t, t') = \begin{bmatrix} \cos \tau & -\sin \tau \\ \sin \tau & \cos \tau \end{bmatrix}, \quad (22)$$

and the phase of the Fourier transformed propagator (20) reduces to elementary integrals,

$$\tilde{G}_W^{\text{pi}}(\gamma'', t''; \gamma', t') = \delta[\gamma'' - \mathbf{M}(t'', t')\gamma'] \exp \left[ \frac{-i\sigma}{3\omega} \int_{\tau'}^{\tau''} d\tau (\alpha' \sin \tau + \beta' \cos \tau)^3 \right].$$

In a reference frame  $\bar{\boldsymbol{\rho}} = (\bar{\eta}, \bar{\xi})$  rotating by  $\tau/2$  with respect to  $\boldsymbol{\rho}$ ,  $\bar{\eta} = \eta \cos(\tau/2) - \xi \sin(\tau/2)$ ,  $\bar{\xi} = \eta \sin(\tau/2) + \xi \cos(\tau/2)$ , the propagator after inverting the Fourier transform takes a particularly transparent form

$$G_W^{\text{pi}}(\bar{\boldsymbol{\rho}}'', t''; \bar{\boldsymbol{\rho}}', t') = \pi \sqrt{f(s)} \kappa(s)^{-2/3} \text{Ai}[\kappa(s)^{-1/3} \bar{\rho}_-] \text{Ai}[\kappa(s)^{-1/3} \bar{\rho}_+], \quad (23)$$

where we abbreviate  $\kappa(s) = \sigma s^3 f(s)/3\omega$ ,  $f(s) = 3s^{-2} - 1$ ,  $s = \sin(\tau/2)$ , and  $\bar{\rho}_{\pm} = (\bar{\eta} \pm \sqrt{f(s)} \bar{\xi})/2$ . The corresponding result for the hyperbolic case  $V''/T'' < 0$ , e.g., close to a quadratic maximum of a cubic potential, is obtained from Eq. (23) by replacing  $f(s) = 3s^{-2} + 1$  and  $s = \sinh(\tau/2)$ .

Equation (23) provides us with a precise geometric outline that complements the features of the Wigner propagator pointed out in the sequel of Eq. (11):

- i. The quantum spot formed by the propagator fills a sector in phase space of opening angle  $\theta = 4 \operatorname{arccot} \sqrt{f(s)}$  (Fig. 3c), rotating by  $\tau/2$  if  $\tau$  is the angle coordinate along the classical trajectory. Its nodes form straight lines running parallel to its sidelines, with separations given by Airy-function zeros (Fig. 3).
- ii. For short scaled time  $\tau \ll 1$ , the oscillatory tail is quasi-one-dimensional,  $\theta \ll 1$ , pointing in the negative  $p$ -direction if  $V''' > 0$  and vice versa, and scales with time as  $\tau^3$ . It is periodic in  $\tau$  with period  $2\pi$  and invariant under time reversal,  $\tau \rightarrow \tau_0 - \tau$ ,  $p \rightarrow -p$ , with respect to  $\tau_0 = 0, \pi$ .
- iii. As expected for a uniform approximation, Eq. (23) resolves the sharp caustics along the outlines of the quantum spot present in the van Vleck approximation (10) (Fig. 3b) into a smooth penumbra (Fig. 3c,d). This restores the correct normalization of the propagator. On the other hand, it restricts the oscillatory pattern to straight node-lines while with Eq. (10), nonlinear deformations owing to higher nonlinearities in the potential can well be reproduced, see Sec. III B.
- iv. The finite weight the propagator (23) achieves in the penumbra zone outside the illuminated region of Eq. (10) can be interpreted as the contribution of complex trajectories. However, we shall not pursue this issue here.

## 2. Perturbation theory from van Vleck approach

A uniform approximation equivalent to Eq. (23) can be obtained through an alternative route which is particularly helpful in order to analyze the asymptotics at weak anharmonicity and at short time and the classical limit for the Wigner propagator: We treat the weak cubic nonlinearity explicitly as a perturbation of an otherwise quadratic Hamiltonian

$$H(p, q) = \frac{p^2}{2m} + \frac{m\omega^2}{2}q^2 + \epsilon q^3, \quad (24)$$

to obtain expressions for the various ingredients of the van Vleck propagator (10) through a perturbation expansion in  $\epsilon$ .

From the perturbed orbits  $\mathbf{r}_\epsilon''(\mathbf{r}', t)$ , we obtain pairs of trajectories  $\mathbf{r}_{\epsilon\pm}''(t) = \mathbf{r}_\epsilon''(\mathbf{r}' \pm \check{\mathbf{r}}'/2, t)$  with initial points displaced by  $\pm\check{\mathbf{r}}'/2$  from  $\mathbf{r}'$ , the corresponding centers  $\bar{\mathbf{r}}_\epsilon''(\mathbf{r}', \check{\mathbf{r}}', t) = (\mathbf{r}_{\epsilon+}'' + \mathbf{r}_{\epsilon-}'')/2$ , and the deviations  $\Delta\mathbf{r}_\epsilon''(\mathbf{r}', \check{\mathbf{r}}', t) = \bar{\mathbf{r}}_\epsilon''(\mathbf{r}', \check{\mathbf{r}}', t) - \bar{\mathbf{r}}_\epsilon''(\mathbf{r}', \mathbf{0}, t)$  of these final midpoints from the endpoint  $\mathbf{r}_\epsilon''(\mathbf{r}', t)$  of the perturbed trajectory starting in  $\mathbf{r}'$ ,

$$\begin{aligned} \Delta p_\epsilon''(\mathbf{r}', \check{\mathbf{r}}', t) &= \frac{3\epsilon}{8\omega} \check{\mathbf{r}}'^t \mathbf{F}_p \check{\mathbf{r}}' + \mathcal{O}(\epsilon^2, t^4), \\ \Delta q_\epsilon''(\mathbf{r}', \check{\mathbf{r}}', t) &= \frac{3\epsilon}{8m\omega^2} \check{\mathbf{r}}'^t \mathbf{F}_q \check{\mathbf{r}}' + \mathcal{O}(\epsilon^2, t^5), \end{aligned} \quad (25)$$

with time-dependent coefficient matrices

$$\mathbf{F}_p = \begin{bmatrix} \frac{2\tau^3}{3} & \tau^2 \\ \tau^2 & 2\left(\tau - \frac{\tau^3}{3}\right) \end{bmatrix}, \quad \mathbf{F}_q = \begin{bmatrix} \frac{\tau^4}{6} & \frac{\tau^3}{3} \\ \frac{\tau^3}{3} & 2\left(\tau^2 - \frac{\tau^4}{6}\right) \end{bmatrix}. \quad (26)$$

Arising from a perturbation expansion of the equations of motion, Eqs. (25, 26) are reliable only up to leading order in  $\tau$ , hence their validity is also restricted in time to  $\tau \ll 2\pi$ . They constitute the classical skeleton of the quantum spot and provide the input for its determinantal prefactor and action.

It is, however, more convenient to express these quantities in terms of  $\Delta\mathbf{r}_\epsilon''$ , the final argument of the propagator relative to the classical trajectory starting in  $\mathbf{r}'$ , instead of the initial displacement  $\check{\mathbf{r}}'$ . By means of a few elementary phase-space transformations that diagonalize simultaneously the two coefficient matrices (26), the pair of quadratic equations (25) can be resolved for  $\check{\mathbf{r}}'$  as a function of  $\Delta\mathbf{r}_\epsilon''$ . We thus obtain the propagator in the form

$$\begin{aligned} G_W^{\text{vV}}(\mathbf{r}'', \mathbf{r}', t) &= \frac{2\pi\hbar\beta}{\left[2\frac{t}{m}\Delta p''^2 - 12\Delta p''\Delta q'' + 12\frac{m}{t}\Delta q''^2\right]^{1/4}} \\ &\times \left\{ \cos \left[ \beta(\Delta r''_+ - \Delta r''_-)^{3/2} \right] + \sin \left[ \beta(\Delta r''_+ + \Delta r''_-)^{3/2} \right] \right\}, \end{aligned} \quad (27)$$

with  $\beta = 2m^{3/4}/3^{3/2}\hbar\epsilon^{1/2}t^{5/4}$  and  $\Delta r''_{\pm} = (1 \mp \sqrt{3})\sqrt{t/m}\Delta p'' \pm 2\sqrt{3m/t}\Delta q''$ . We identify the cosine term in Eq. (27) as the contribution of the pair of hyperbolic trajectories (saddles of the action, Fig. 3e) and the sine term as the elliptic contribution (extrema, Fig. 3f), cf. remark (vi) after Eq. (11) and Fig. 2c.

Unfortunately, Eq. (27) becomes spurious precisely in the limit  $\epsilon \rightarrow 0$  for which it has been devised, since in this limit, the stationary points of the action coalesce and the stationary-phase approximation underlying Eq. (27) breaks down. The problem can be fixed, however, in a straightforward manner: Since the action in Eq. (7) is odd in the integration variable  $R$  and the two known trajectory pairs entering Eq. (27) mark its four stationary points  $\mathbf{R}_{--} = -\mathbf{R}_{++}$  and  $\mathbf{R}_{-+} = -\mathbf{R}_{+-}$  (Fig. 2c), corresponding resp. to the elliptic and hyperbolic pairs, we can uniquely reconstruct an effective action that contains only linear and cubic terms in  $R$  (Fig. 2c) and thus permits an exact evaluation of the  $R$ -integration. The result (cf. Fig. 3c), replacing Eq. (27), reads

$$G_{\text{W}}^{\text{pi}}(\mathbf{r}'', \mathbf{r}', t) = \frac{4\sqrt{3}}{\alpha^{2/3}} \text{Ai}\left(\frac{\Delta r''_{-}}{\alpha^{1/3}}\right) \text{Ai}\left(\frac{\Delta r''_{+}}{\alpha^{1/3}}\right), \quad (28)$$

with  $\alpha = 3\epsilon\hbar^2 t^{5/2} m^{-3/2}$  and  $\Delta r''_{-}, \Delta r''_{+}$  as above. It follows from Eq. (23) as a short-time approximation, to leading order in  $\tau$ . Equation (27), in turn, is recovered if we replace the Airy functions by their asymptotics for large negative argument [64],  $\text{Ai}(-x) \rightarrow \pi^{-1/2}(\frac{3}{2})^{1/4} x^{-3/8} \sin(\frac{2}{3}x^{3/2} + \frac{\pi}{4})$ .

Equation (28) has been obtained combining perturbation theory with semiclassics on the level of the van Vleck propagator augmented by a uniform approximation—a route that might appear less systematic and controlled than the access through phase-space path integration that led to Eq. (23). Its virtue, though, lies in the fact that it is based on trajectory pairs, hence readily extends to a higher number of degrees of freedom, while this is far from obvious in the case of path integration. This feature together with its simplicity and the fact that it is adapted to short propagation time suggests Eq. (28) as a suitable choice for on-the-fly molecular-dynamics applications [27, 28].

### 3. Asymptotics $\epsilon \rightarrow 0$ , $\hbar \rightarrow 0$ , $t \rightarrow 0$

As pointed out the discussion of Eq. (11), the semiclassical Wigner propagator replaces the Liouville propagator by a smooth quantum spot only if the potential is not purely harmonic.



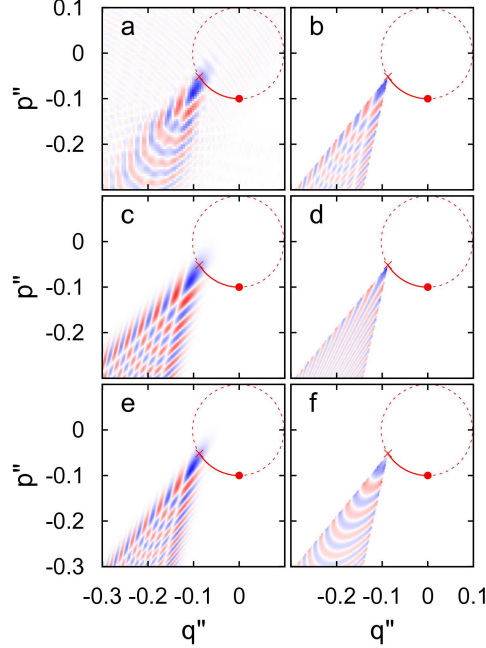


FIG. 3: Different versions of the Wigner propagator for a harmonic potential with weak cubic anharmonicity as a function of the final phase-space coordinates  $(q'', p'')$  at a scaled time  $\omega t = \pi/3$ : Wigner propagator in the semiclassical approximation (23) based on the exact quantum result (37) (panel a), the van Vleck approximation (27) (b), phase-space path integration (c), and short-time version (28) of the same approach (e). Panels d,f are contributions to Eq. (27) corresponding to hyperbolic (cosine term, d) and elliptic (sine term, f) trajectory pairs, respectively, cf. Fig. 2b,c. Parameter values are  $\hbar = 0.01$ ,  $\epsilon = 0.2$ ,  $m = 1$ ,  $\omega = 1$ . The underlying classical trajectory (red line in all panels) has been launched at  $(q', p') = (0, -0.1)$ . Color code ranges from red (negative) through white (zero) through blue (positive).

It should converge to the Liouville propagator for vanishing anharmonicity. Indeed, invoking the asymptotic expression  $\lim_{\kappa \rightarrow 0} \kappa^{-1} \text{Ai}(x/\kappa) = \delta(x)$  [65] for the Airy functions in Eq. (23), we find for  $\alpha \rightarrow 0$ ,  $G_W(\mathbf{r}'', \mathbf{r}', t) = 4\sqrt{3}\delta(\Delta r''_-)\delta(\Delta r''_+)$ . Separating  $\Delta p''$  and  $\Delta q''$  in the arguments of the delta functions, this proves to be equivalent to  $G_W(\mathbf{r}'', \mathbf{r}', t) = \delta(\Delta \mathbf{r}'')$ , the classical Liouville propagator. Considering the dependence of  $\alpha$  on  $\epsilon$ ,  $\hbar$ , and  $t$ , this includes the classical limit (for subtleties of this limit for Wigner functions and their propagation, see [66]) and the limit  $t \rightarrow 0$ . Moreover, the powers 1, 2, and 2.5, respectively, with which  $\epsilon$ ,  $\hbar$ , and  $t$  appear in  $\alpha$ , indicate a hierarchy of the corresponding limits: At finite  $\hbar$ , the smooth quantum spot already collapses to a delta function in the limit of weak anharmonicity, i.e.,

for a quantum harmonic oscillator. And even at finite  $\epsilon$ , taking into account the different scaling with time of  $\Delta q''$  and  $\Delta p''$  as they enter Eq. (27), the lateral ( $\bar{\xi}$ ) extension of the quantum spot disappears first with  $t \rightarrow 0$  while its longitudinal ( $\bar{\eta}$ ) dimension (in  $\Delta p''$ -direction) scales with  $t$  as it does with  $\epsilon$ .

### III. NUMERICAL RESULTS

#### A. Models

##### 1. Morse oscillator

We choose the Morse oscillator for a detailed study of semiclassical Wigner propagation for two reasons: Above all, being prototypical for strongly anharmonic molecular potentials and correspondingly complex dynamics [67–70], it is a widely used benchmark for numerical methods in this realm [4, 21, 71–73]. Secondly, the Morse oscillator has the remarkable advantage, shared only with very few other potentials, that closed analytical expressions are available not only for its energy eigenstates [74] but even for their Wigner representations [71], a feature that greatly facilitates the comparison with exact quantum-mechanical results [43, 71, 75–78] and hence provides a solid basis for an objective test of the performance of semiclassical approximations to the propagator.

The one-dimensional Morse potential [74]

$$V_{\text{Morse}}(q) = D(1 - e^{-aq})^2 \quad (29)$$

is determined by the depth  $D$  and inverse width  $a$  of the potential well. Quantum-mechanically, its spectrum is discrete for  $0 < E < D$  and continuous for  $E > D$ . The number of bound states  $|\alpha\rangle$  is given (up to  $O(1)$ ) by the parameter  $\lambda = \sqrt{2mD}/a\hbar$ , to be interpreted as an inverse Planck's constant in natural units. Analytical expressions in terms of Laguerre polynomials are available for the eigenfunctions  $\psi_\alpha(q) = \langle q|\alpha\rangle$ , see Refs. [71, 74]. Applying the Weyl transform (1) to  $\hat{\rho} = |\alpha\rangle\langle\alpha|$  then leads to the corresponding Wigner eigenfunctions  $W_{\alpha\alpha}(\mathbf{r})$  [71]. Exact solutions for the continuum states, on the other hand, are not known. Numerical evidence indicates, however, that the error caused by their omission in the basis set underlying quantum calculations of the time evolution is acceptable as long as the energy does not come too close to the threshold  $E = D$ .

## 2. Quartic double well

The quartic double-well potential is in many respects complementary to the Morse oscillator. From a phenomenological point of view, it is the standard model for the study of coherent tunneling, and therefore constitutes a particularly hard problem for semiclassical propagation. Technically, it is characterized by the absence of a continuum, which facilitates quantum calculations. At the same time, no analytical expressions for its eigenfunctions are known.

To begin with, define the quartic double-well potential as  $V(x) = -m\omega^2 x^2/4 + m^2\omega^4 x^4/64E_b$ , where  $\omega$  is the oscillation frequency near the minima at  $x_{\pm} = \pm\sqrt{8E_b/m\omega^2}$  and  $E_b$  their depth. In natural units  $q = \sqrt{m\omega/\hbar}x$  and  $\tau = \omega t$ , the Schrödinger equation reads

$$i\frac{\partial}{\partial t}|\psi\rangle = \hat{H}|\psi\rangle, \quad \hat{H}(\hat{p}, \hat{q}) = \frac{\hat{p}^2}{2} - \frac{\hat{q}^2}{4} + \frac{\hat{q}^4}{64\Delta}. \quad (30)$$

Its only parameter, the dimensionless barrier height  $\Delta = E_b/\hbar\omega$ , measures approximately the number of tunneling doublets, half the number of eigenstates below the barrier top.

Eigenvalues and eigenfunctions underlying the exact quantum calculations shown in the sequel have been obtained in a basis of harmonic-oscillator eigenstates, with unit frequency and centered at  $q = 0$ .

### B. Propagating delta functions: the propagator as a stand-alone quantity

To our best knowledge, no detailed account of the propagator of the Wigner function as a quantity of its own right has been published to date, except for the recent Ref. [56]. Indeed, it is inaccessible to semiclassical approximation schemes based on Gaussian smoothing. We therefore find it appropriate to illustrate its basic properties with data obtained for the two models featured in this section. Moreover, the interference pattern characterizing the Wigner propagator is a sensitive diagnostic for the performance of the different semiclassical approximations we are proposing. In addition, an analysis of the propagator allows to assess by mere inspection the validity of propagation schemes based on non-classical but deterministic trajectories [43–47], see Sec. III D.

The naked propagator is equivalent to the time evolution of a delta function as initial Wigner function, which is not an admissible Hilbert-space element. Notwithstanding, since

Wigner functions are measurable, e.g., through quantum-state tomography [79], so is the propagator, under weak conditions [63], by unfolding the final Wigner function from the initial one, which adds legitimacy to considering the propagator as a stand-alone quantity.

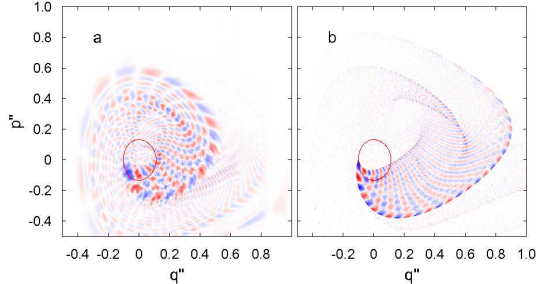


FIG. 4: Van-Vleck-based semiclassical Wigner propagator (10, 11) (b) and corresponding exact quantum result (37) (a) as a function of the final phase-space coordinates  $(q'', p'')$  for the Morse oscillator (29) at intermediate energy  $E = 0.018$  at  $t = 10$ , approximately the period of the underlying classical orbit (red line). Parameters are  $m = 0.5$ ,  $D = 1$ ,  $a = 1.25$ ,  $\hbar = 0.005$ , the initial point is  $(q', p') = (-0.1, 0)$ . Color code as in Fig. 3.

The linear checkerboard structure of the quantum spot appearing in Fig. 3 is owed to the cubic anharmonicity of the potential to which the figure refers (its poor resolution in the quantum result, panel a, is a numerical artefact). In Fig. 4, we contrast it with data for the Morse oscillator, at an intermediate energy  $E = 0.018D$  where the nonlinearity is already considerable, and after a propagation time  $\omega t = 10$  of the order of the period of the underlying classical orbit. The pattern of Fig. 3 can still be discerned but is severely distorted. The nodelines are now strongly curved, and the pattern even folds over, giving rise to a phase-space swallow-tail catastrophe. The van-Vleck-based semiclassical propagator (10, 11) (panel b) captures this complicated structure surprisingly well. The path-integral-based approximation, by contrast, does not reproduce these distortions (not shown).

Figure 5 shows a similar comparison for the quartic double well, at an energy above the barrier top. Here, the interference pattern is even more complex than in Fig. 4. While the van-Vleck-based propagator does not agree with the quantum calculation in the intricate fine details of the oscillatory fringes, it correctly reproduces much of the more global features of the distribution. For an account of its performance at energies below the barrier top, see Sec. III F.

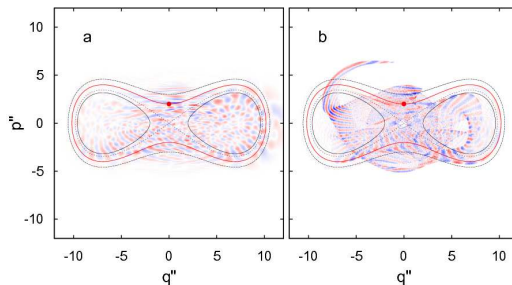


FIG. 5: As Fig. 4 but for the quartic double well (30) with  $\Delta = 6$  at energy  $E = 2$  above the barrier at  $t = 5$ , approximately the period of the underlying classical orbit (red line). The initial point is  $(q', p') = (0, 2)$ . Color code as in Fig. 3.

### C. Propagating Gaussians

Gaussian initial states deserve their ubiquity not only for their unique physical properties, exemplified by coherent states. In the context of the Wigner representation, Gaussians gain special relevance as they constitute the only admissible Wigner functions that are positive definite and therefore can be interpreted in probabilistic terms [80]. They have achieved a fundamental rôle for semiclassical propagation as they provide a natural smoothing which allows to reduce the time evolution of an entire phase-space region to the propagation along a single classical trajectory.

By difference to Gaussian-wavepacket propagation and semiclassical IVRs, however, the semiclassical Wigner propagator does not involve any smoothing by construction and thus allows to time-evolve arbitrary initial states, Gaussian or not. A more specific question is then how semiclassical approximations to it operate on the space of Gaussian phase-space distributions. We find that they generally transform them into a broader class of functions which, in view of the above theorem, can no longer remain positive definite.

Define Gaussians in phase space [81] by

$$W(\mathbf{r}) = \frac{\sqrt{\det \mathbf{A}}}{(2\pi\hbar)^f} \exp \left[ -\frac{(\mathbf{r} - \mathbf{r}_0)^t \mathbf{A} (\mathbf{r} - \mathbf{r}_0)}{2\hbar} \right]. \quad (31)$$

The  $2f \times 2f$  covariance matrix  $\mathbf{A}$  controls size, shape, and orientation of the Gaussian centered in  $\mathbf{r}_0 = (\mathbf{p}_0, \mathbf{q}_0)$ . The more specific class of minimum-uncertainty Gaussians, equivalent to Wigner representations of coherent states [37], is characterized by  $\det \mathbf{A} = 1$ . In what

follows, in two dimensions  $\mathbf{r} = (p, q)$ , we choose  $\mathbf{A} = \text{diag}(1/\gamma, \gamma)$ , so that

$$W(\mathbf{r}) = \frac{1}{\pi\hbar} \exp \left[ -\frac{(p - p_0)^2 + \gamma^2(q - q_0)^2}{\gamma\hbar} \right], \quad (32)$$

equivalent to a position-space wave function [81]  $\psi(\mathbf{q}) = (\pi\hbar)^{-f/4} \exp[-\frac{\gamma}{2\hbar}|q - q_0|^2 + \frac{i}{\hbar}\mathbf{p}_0 \cdot (\mathbf{q} - \mathbf{q}_0)]$ .

### 1. Autocorrelation functions

A standard interface between dynamical and spectral data, autocorrelation functions have a wide range of applications in atomic and molecular physics and provide a robust and easily verifiable assay of the accuracy and efficiency of propagation methods. The overlap  $C_\psi(t) = \langle \psi(t) | \psi(0) \rangle$  for an initial state  $|\psi(0)\rangle$  upon squaring readily translates into an expression in terms of the Wigner representation  $W_\psi(\mathbf{r})$  of that state,  $|C_\psi(t)|^2 = (2\pi\hbar)^f \int d^{2f}r W_\psi(\mathbf{r}, 0)W_\psi(\mathbf{r}, t)$ , or, involving the propagator explicitly,

$$|C_\psi(t)|^2 = (2\pi\hbar)^f \int d^{2f}r'' \int d^{2f}r' W_\psi(\mathbf{r}'', 0)G_W(\mathbf{r}'', \mathbf{r}', t)W_\psi(\mathbf{r}', 0). \quad (33)$$

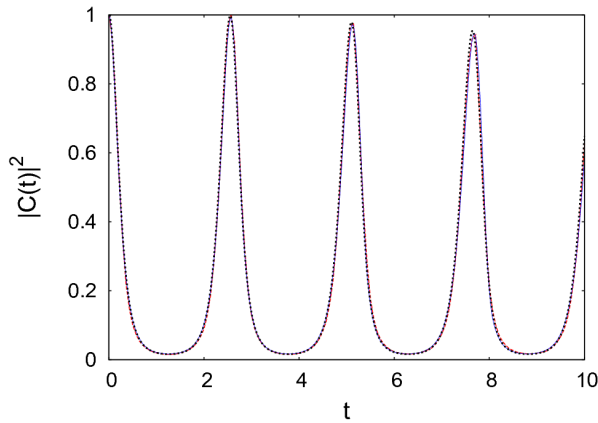


FIG. 6: Autocorrelation function (33) for a Gaussian initial state (31) in a Morse potential (29), for the semiclassical approximation (10, 11) (dashed line, red), compared to an exact quantum (Eq. (37), full line, blue) and a classical calculation (Eq. (12), dotted, black) of the Wigner propagator. Parameter values are  $m = 0.5$ ,  $D = 1$ ,  $a = 1.25$ ,  $\hbar = 0.005$ , the initial centroid is  $(q_0, p_0) = (-0.1, 0)$ .

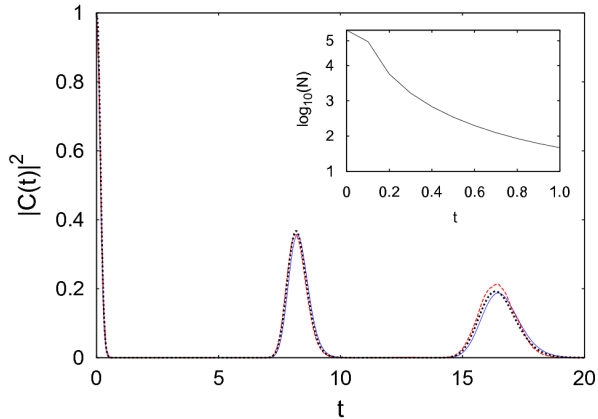


FIG. 7: As Fig. 6 but for a quartic double well (30) with  $\Delta = 6$  at an energy  $E = 1.0026$  above the barrier top. The initial centroid of the Gaussian is  $(q_0, p_0) = (4, 7)$ . Inset: Nonconservation of the norm  $N$  for the same propagation process but without interspersed normalization steps.

In Fig. 6, we compare the autocorrelation functions (33) for the Morse oscillator with a Gaussian initial state (31) as obtained by an exact quantum calculation (full line) to the semiclassical approximation (10, 11) (dashed) and the classical propagator (12) (dotted) at an intermediate energy. Over the roughly four periods of the classical trajectory monitored, the agreement is impressive. Figure 7 is an analogous comparison but for the quartic double-well potential. Here, the discrepancy between semiclassical and quantum data is slightly more significant.

In order to obtain the data underlying Figs. 6, 7, it was necessary to periodically renormalize the propagator, compensating for a lack of norm conservation as is notorious for van-Vleck-based approximations [82]. In Fig. 7 (inset), we are monitoring the loss of the norm of the final Wigner function for a typical run of the propagator (10, 11) without renormalization in the quartic double well over a fraction of the period of the underlying classical orbit.

## 2. Resolving phase-space structures

More detailed information on the performance of propagators and reasons for their possible failure than is contained in autocorrelation functions can be extracted from the full phase-space structures of propagated Gaussians. In particular in strongly nonlinear sys-

tems, the degree to which a semiclassical propagator is able to reproduce deviations of the time-evolved states from Gaussians is a sensitive measure of its quality.

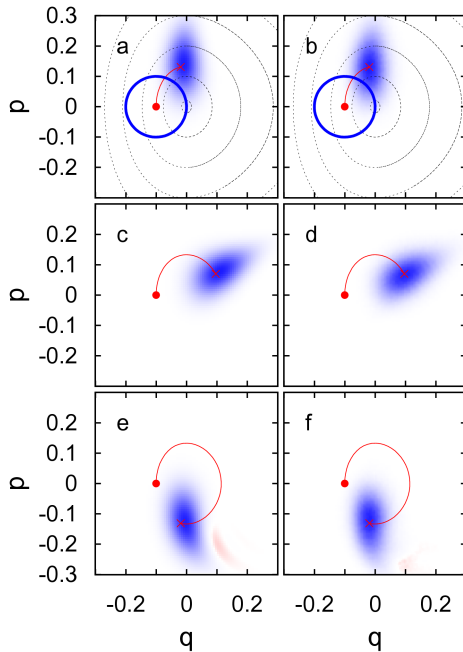


FIG. 8: Time evolution of a state prepared as a minimum-uncertainty Gaussian (32) (bold blue circle in panels a,b is its contour enclosing a Planck cell) in the Morse potential (29) (black contour lines in panel a) for the semiclassical approximation (10, 11) (right column), compared to an exact quantum calculation (37) (left), at times  $t = 0.5072$  (panels a,b),  $1.0144$  (c,d),  $2.0288$  (e,f). The full red line is the classical orbit of the initial centroid  $(q_0, p_0) = (-0.1, 0)$ . Parameter values are  $m = 0.5$ ,  $D = 1$ ,  $a = 1.25$ ,  $\hbar = 0.005$ . Color code as in Fig. 3.

Such deviations are unmistakable in Fig. 8, a series of snapshots of the time evolution of an initially Gaussian state under the same conditions as for the autocorrelation function depicted in Fig. 6. The asymmetric droplet shape of the distribution, notably in panels c to f, is not compatible with a linearly deformed Gaussian, but is immediately explained by the form of the underlying propagator on the centroid trajectory, superimposed on the evolved distribution at the same time (Fig. 9). The non-elliptic shape is therefore a consequence of the strongly anharmonic potential. In Fig. 8, panels e,f, we even observe fringes where the distribution takes on negative values. Unavoidable for non-Gaussian Wigner functions [80], this behavior appears even more conspicuous in Fig. 10, analogous to Fig. 8 but for a quartic



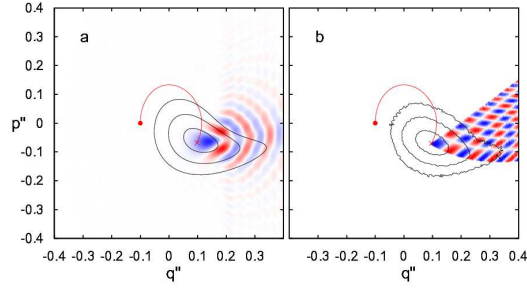


FIG. 9: Same as Figs. 8c,d but comparing the time-evolved Gaussian (contour lines) to the respective propagator (10, 11) on the centroid orbit (red) at the same time  $t = 1.0144$ . Color code as in Fig. 3.

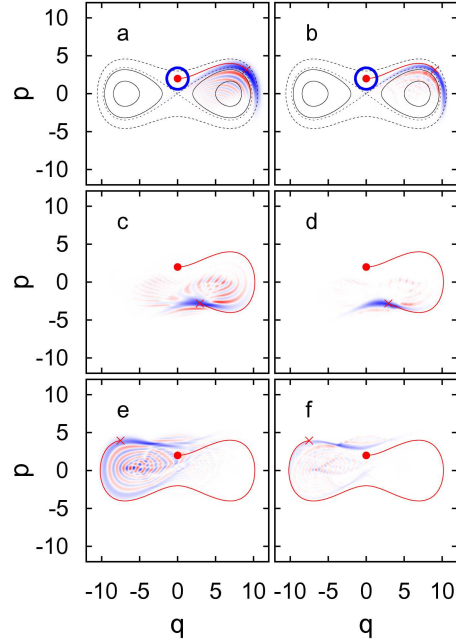


FIG. 10: As Fig. 8 but for the quartic double well (30) with  $\Delta = 6$  at times  $t = 3$  (panels a,b), 9 (c,d), 15 (e,f). The initial centroid is  $(q_0, p_0) = (0, 2)$ . Color code as in Fig. 3.

double well potential. At the same time, the resolution of these structures is relatively poor, owing to the reduced density of classical trajectories used in the calculation towards the periphery of the initial distribution.

A more quantitative account of this feature is obtained considering the semiclassical propagator (23). Folding Airy functions with initial minimum-uncertainty Gaussians leads into

a wider function space of polynomials of up to cubic order in the exponent and, in semiclassical Wigner propagation, replaces the (frozen, thawed, etc.) Gaussians constituting the framework of Gaussian-wavepacket propagation [19–23]. It ranges from strongly distorted, oscillatory distributions in the “deep quantum regime” to near Gaussians in the semiclassical limit.

#### D. Propagating stationary states

Propagating energy eigenstates of a quantum system may appear a trivial task. For the propagation of Wigner functions, however, there is more to gain than just a check of norm conservation, as explained in a remarkable work by Lee and Scully [43]. They argue that, while for a system with anharmonic potential a phase-space flow along classical trajectories cannot reproduce the quantum dynamics, at least in the case of energy eigenstates they may be replaced by another type of characteristic: Evidently, Wigner functions associated to eigenstates are invariant under a flow that follows their contour lines, suggesting the latter as a kind of “Wigner trajectories” to replace the classical ones for finite  $\hbar$ .

In the present subsection, we confront their proposal with semiclassical Wigner propagation along pairs of classical trajectories, taking advantage of the fact that also Ref. [43] is based on a study of the Morse oscillator. We not only find that our method describes the quantum evolution of eigenstates to high accuracy in terms of autocorrelations (far better than [43]) but even present convincing arguments why the very concept of a quantum phase-space flow along “Wigner trajectories” is misleading.

In Fig. 11 we contrast the contours of the second excited eigenstate of the Morse oscillator in Wigner representation [71] with classical trajectories for the same system. At this point, it is not even clear which contour to compare with which trajectory. As a reasonable choice which becomes compelling in the classical limit, for a given eigenstate  $|\alpha\rangle$  we focus on the classical trajectory at  $E = E_\alpha$ . Along this “quantizing” orbit, the corresponding Wigner eigenfunctions exhibit a narrow ridge, to be chosen as the relevant contour. We find that the classical trajectory roughly follows the contour line but deviates in quantitative detail.

We would expect semiclassical approximations to improve systematically on mere classical propagation. Figure 11 illustrates how this is achieved by propagating along midpoints of non-identical classical trajectory pairs: Keeping the initial point  $\mathbf{r}'$  on a given Wigner contour

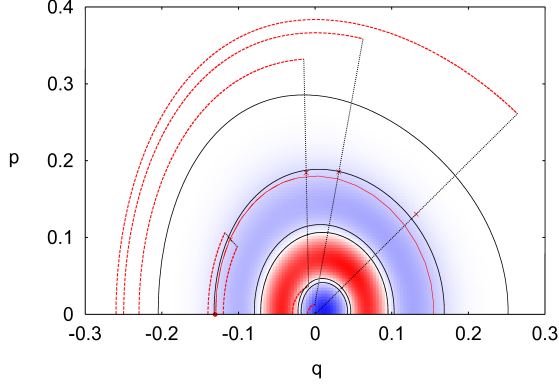


FIG. 11: Wigner representation of the second excited state of the Morse oscillator [71] (black contour lines and color code as in Fig. 3), compared to the classical orbit  $\mathbf{r}_{E_2}^{\text{cl}}(t)$  at the corresponding eigenenergy  $E_2$  (full red line) and to midpoint paths  $\bar{\mathbf{r}}_j(t) = [\mathbf{r}_{j-}^{\text{cl}}(t) + \mathbf{r}_{j+}^{\text{cl}}(t)]/2$  for pairs of classical trajectories  $\mathbf{r}_{j\pm}^{\text{cl}}(t)$  (dashed red lines), with common initial midpoint  $\bar{\mathbf{r}}' = \mathbf{r}_{E_2}^{\text{cl}}(0)$  but increasing initial separation  $\check{\mathbf{r}}'_j \equiv (\check{p}'_j, \check{q}'_j) = \mathbf{r}'_{j+} - \mathbf{r}'_{j-}$  with  $\check{p}'_j = 0$  and  $\check{q}'_j = 0.002, 0.2, 0.24, 0.26$  (see text). Parameter values are  $m = 0.5$ ,  $D = 1$ ,  $a = 1.25$ ,  $\hbar = 0.005$ .

fixed, we increase the initial separation  $\check{\mathbf{r}}'_j = \mathbf{r}'_{j+} - \mathbf{r}'_{j-}$  of the trajectory pairs launched in  $\mathbf{r}'_{j\pm}$ . While for  $\check{\mathbf{r}}' = 0$  (classical trajectory) the deviation from the contour line is large, the midpoint paths  $\bar{\mathbf{r}}_j(t) = [\mathbf{r}_{j-}(t) + \mathbf{r}_{j+}(t)]/2$  indeed appear to move towards the Wigner contour with increasing  $\check{\mathbf{r}}'$ . However, they do not approach it asymptotically but continue shifting further past the Wigner contour, indicating that it plays no particular rôle for quantum time evolution in phase space, not even of eigenstates.

In fact, semiclassical Wigner propagation generally does not reduce to a deterministic phase-space flow, not along classical nor along modified (quantum) trajectories. In Fig. 12 we show the quantum spot formed by the Wigner propagator for the same initial conditions as in Fig. 11. As in similar plots throughout this paper, it appears as a smooth distribution that cannot be replaced by a delta function, neither on the classical trajectory *nor on the Wigner contour*. It is perhaps surprising but by no means inexplicable that this propagator, while reshuffling the Wigner distribution in phase space, nonetheless keeps the Wigner eigenfunction invariant.

This is confirmed by Fig. 13. We are plotting the autocorrelation function for the eigenstate  $W_{00}(\mathbf{r})$  as initial state, which in this case coincides with the norm, propagated with

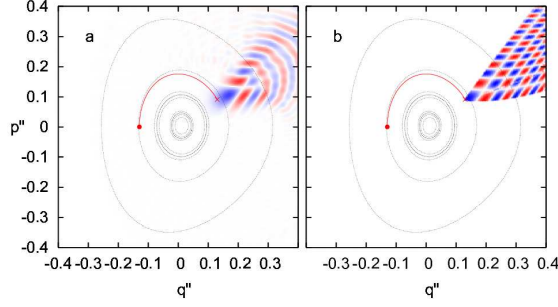


FIG. 12: Van-Vleck based Wigner propagator (10, 11) (panel b) and corresponding exact quantum result (37) (a) for the Morse potential (29) as a function of the final phase-space coordinates  $(q'', p'')$ , at  $t = 1.5216$ . The initial point  $\mathbf{r}' = \mathbf{r}_{E_2}^{\text{cl}}(0)$  is the same as in Fig. (11). They are compared to the classical orbit  $\mathbf{r}_{E_2}^{\text{cl}}(t)$  (bold line) and the contour of the Wigner eigenfunction  $W_{22}(\mathbf{r})$  (grey), cf. Ref. [71], passing through  $\mathbf{r}_{E_2}^{\text{cl}}(0)$ . Parameter values are  $m = 0.5$ ,  $D = 1$ ,  $a = 1.25$ ,  $\hbar = 0.005$ . Color code as in Fig. 3.

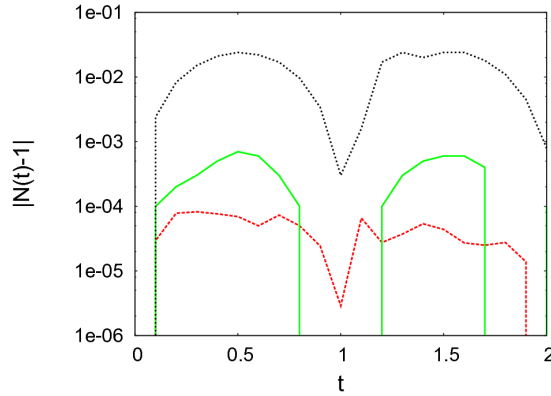


FIG. 13: Accuracy of the autocorrelation function for the ground state  $W_0(\mathbf{r})$  of the Morse oscillator (equivalent to norm conservation) propagated with the semiclassical approximation (10, 11) to the Wigner propagator (dashed line, red), a deterministic flow along Wigner contours (full line, green), and the classical Liouville propagator (12) (dotted, black). Parameter values are  $m = 0.5$ ,  $D = 0.15$ ,  $a = 1$ ,  $\hbar = 1.0$ .

the semiclassical Wigner propagator (10, 11), and find deviations of the order of  $10^{-5}$  only, as compared to the range of  $10^{-4}$  for propagation along Wigner contours and  $10^{-3}$  for mere classical Wigner dynamics. Moreover, in Fig. 14 we compare the semiclassically propagated state at  $t = 10$  with the initial state. There is no visible difference. We conclude that

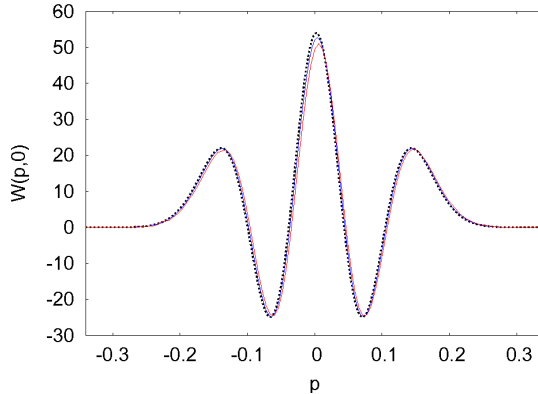


FIG. 14: Cross section at  $p = 0$  of the Wigner eigenfunction  $W_{22}(\mathbf{r})$ , cf. Ref. [71], before (full line, blue) and after propagation through a time  $t = 10$  with the semiclassical approximation (10, 11) to the Wigner propagator (dashed line, red) and the classical Liouville propagator (12) (dotted, black).

even in the case of propagating Wigner eigenstates, an acceptable semiclassical approximation to the Wigner propagator must not only propagate along non-classical paths but differ significantly from a delta function on whatever single trajectory, classical or “quantum”.

### E. Propagating Schrödinger cat states

The propagation of Schrödinger cat states [39] is certainly not a standard task of molecular dynamics. Yet it is relevant for the field in various respects: Schrödinger cats are a paradigm of quantum coherence and embody the essence of entanglement in a simple setting. They allow us to test the performance of propagation methods in this particular respect in an objective manner, as the separation of the superposed alternatives and thus the wavelength of the corresponding interference pattern can be precisely controlled. In fact, the classic double-slit experiment referred to in Ref. [40] to elucidate the challenge quantum coherence poses to semiclassical propagation is just a contemporary embodiment of a Schrödinger cat, albeit before this term became popular. Finally, a timely, if fancy, application of this notion are implementations of quantum computation in medium-size molecules [83].

We here consider the propagation of Schrödinger cats prepared as the superposition of two coherent states, cf. Eq. (32), with variable separation  $d$  initially in position. In the

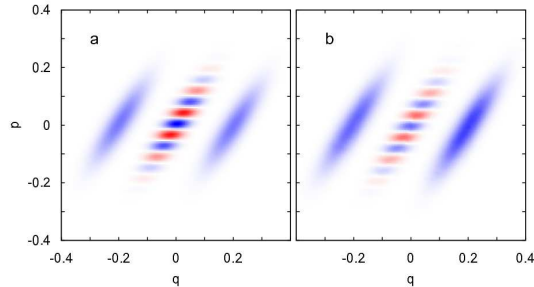


FIG. 15: Schrödinger-cat states time-evolved (34) in the Morse potential (29) at  $t = 0.3$ , for propagation with the semiclassical approximation (10, 11) to the Wigner propagator (panel b) as compared to an exact quantum calculation (37) (a). Parameter values are  $m = 0.5$ ,  $D = 1$ ,  $a = 0.25$ ,  $\hbar = 0.005$ . The initial midpoint and separation, resp., of the Schrödinger cat are  $(q_0, p_0) = (0.3, 0)$ ,  $d = 0.2$ . Color code as in Fig. 3.

Wigner representation, this amounts to

$$W_{\text{cat}}(\mathbf{r}) = W_{-}(\mathbf{r}) + W_{+}(\mathbf{r}) + W_{\times}(\mathbf{r}), \quad (34)$$

where  $W_{\pm}(\mathbf{r}) = \exp\{-[p_{\pm}^2 + \gamma^2 q_{\pm}^2]/\gamma\hbar\}/\pi$ ,  $\mathbf{r}_{\pm} = \mathbf{r} - [\mathbf{r}_0 \pm (0, d)]$ , while  $W_{\times}(\mathbf{r}) = \exp\{-[(p - p_0)^2 + \gamma^2(q - q_0)^2]/\gamma\hbar\} \times \cos[2(p - p_0)d/\hbar]$  encodes the quantum coherence in terms of “sub-Planckian” oscillations of wavelength  $\hbar/d$  in  $p$  [39]. This initial state is propagated with the semiclassical propagator (10, 11) in the Morse potential from the same initial position  $\mathbf{r}_0$  as in Fig. 8. The result is compared in Fig. 15 to the exact quantum calculation. Apart from minor deviations in the shape of the Gaussian envelope, the interference pattern is faithfully reproduced. This is not surprising in view of the trajectory-pair construction underlying our semiclassical approximation:

It is instructive to see why propagating along the two classical trajectories of the respective centroids of the two “classical” Gaussians  $W_{\pm}(\mathbf{r})$  already reproduces essentially the sub-Planckian oscillations. The propagator launched from the centroid  $\mathbf{r}_0$  of  $W_{\times}(\mathbf{r})$  then comprises two terms,  $G_{\text{W}}(\mathbf{r}'', \mathbf{r}_0, t) = G_{\text{W}0}(\mathbf{r}'', \mathbf{r}_0, t) + G_{\text{W}\times}(\mathbf{r}'', \mathbf{r}_0, t)$ . According to Eqs. (10, 11), the first one, propagating along  $\mathbf{r}^{\text{cl}}(\mathbf{r}_0, t)$ , bears no oscillating phase factor and therefore practically cancels upon convolution with the strongly oscillatory  $W_{\times}(\mathbf{r}')$ . The second one, by contrast, is the contribution of the two centroid orbits  $\mathbf{r}^{\text{cl}}(\mathbf{r}_{\pm}, t)$  forming a pair of non-identical trajectories. It travels along the non-classical midpoint path  $\bar{\mathbf{r}}_{\times}(t) = (\mathbf{r}^{\text{cl}}(\mathbf{r}_{-}, t) + \mathbf{r}^{\text{cl}}(\mathbf{r}_{+}, t))/2$  and carries a factor  $\sim \cos[(2/\hbar)(\mathbf{r}_{+} - \mathbf{r}_{-}) \wedge \mathbf{r}'] = \cos[2dp'/\hbar]$

which couples resonantly to the oscillations in  $W_{\times}(\mathbf{r}')$ .

## F. Tunneling

Tunneling is to be regarded a quantum coherence effect “of infinite order in  $\hbar$ ” [84]. One therefore does not expect a particularly good performance of semiclassical methods in its description, despite various efforts that have been made to improve them in this respect. Above all, the complexification of phase space provides a systematic approach to include tunneling in a semiclassical framework [5, 85, 86]. Here, by contrast, we restrict ourselves to real phase space, in order not to lose the valuable close relationship between Wigner and classical dynamics. Even so, we expect that in this framework tunneling can be reproduced to a certain degree [87, 88]. To be sure, Wigner dynamics (in real phase space) is exact for harmonic potentials. This includes parabolic barriers and hence a specific case of tunneling, as pointed out and explained by Balazs and Voros [87]: Since the Wigner propagator invariably follows classical trajectories, the explanation rather refers to the initial condition in Wigner representation: Owing to quantum uncertainty, it spills over the separatrix even if it is concentrated at negative energies, and thus is transported in part with the classical flow to the other side of the barrier.

This is to be considered as a fortunate exception, though. Other, more typical cases involving genuine quantum effects, as in particular coherent tunneling between bound states as we are considering it here, are not so readily accessible to semiclassical Wigner dynamics. Quantum tunneling in the Wigner representation, specifically for localized scattering potentials, has been studied at depth in [49, 89], however without indicating a promising perspective for semiclassical approximations. We are in a slightly more favorable situation as the concept of propagation along trajectory pairs provides a viable option how to reproduce tunneling by means of a semiclassical Wigner propagator: As illustrated in Fig. 16 (inset), it is trajectory pairs with sufficiently separated initial points, probing regions in phase space classically inaccessible to one another, which lead to transport along classically forbidden paths.

Figure 16 is the autocorrelation function for a Gaussian initial state prepared at an energy slightly below the barrier top of the quartic double well (30). The semiclassical Wigner propagator (10, 11) reproduces the revivals but exaggerates their amplitude. This significant

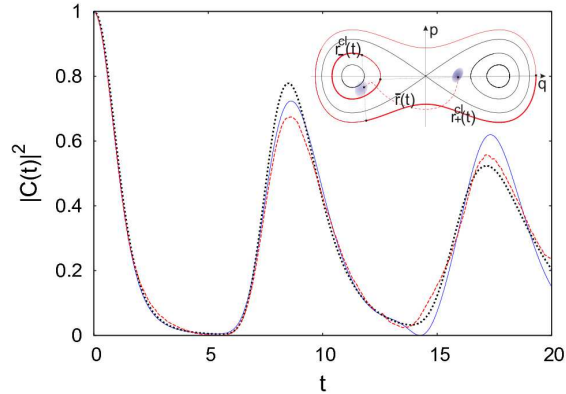


FIG. 16: Autocorrelation function (33) for a Gaussian initial state (31) in a quartic double well (30) with  $\Delta = 6$  at an energy  $E = -0.958333$  below the barrier top, for the semiclassical approximation (10, 11) (dashed line, red), compared to an exact quantum (Eq. (37), full line, blue) and a classical calculation (Eq. (12, dotted, black) of the Wigner propagator. The initial centroid of the Gaussian is  $(q_0, p_0) = (2, 0)$ . Inset: Semiclassical description of coherent tunneling in terms of trajectory pairs, in the framework of the van-Vleck based Wigner propagator (10, 11). A wavepacket initially prepared near the right minimum of a double-well potential (blue patch) is transported along a non-classical midpoint path  $\bar{\mathbf{r}}(t) = (\mathbf{r}_-^{\text{cl}}(t) + \mathbf{r}_+^{\text{cl}}(t))/2$  (dashed red line) into the opposite well if the two classical orbits  $\mathbf{r}_\pm^{\text{cl}}(t)$  (full red lines) underlying this path are sufficiently separated initially, e.g.,  $\mathbf{r}_+^{\text{cl}}$  on the same side but above the barrier,  $\mathbf{r}_-^{\text{cl}}$  within the opposite well. Black lines indicate other contours of the potential and the separatrix.

deviation surprises as it *overestimates* quantum effects. The reasons become clearer upon analyzing the full phase-space distribution for the propagated state, Fig. 17, at a time corresponding to the right edge of Fig. 16. In terms of global features of the distribution, the agreement of the semiclassical (left) with the quantum result (right) is good, remarkably even in phase-space regions classically inaccessible from the initial distribution. However, while the fine fringes of the quantum distribution reaching out into the opposite well do appear in the semiclassical result, their relative weight is not correctly reproduced. This is partially explained by the incorrect balance between central peak and oscillatory tail in the semiclassical propagator. Moreover, with  $\Delta = 6$ , we are in a marginally semiclassical regime and cannot expect an optimal performance of the van-Vleck-based Wigner propagator.



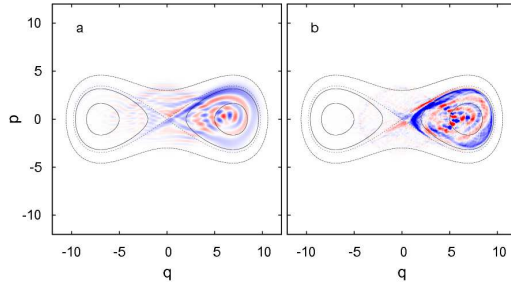


FIG. 17: Time-evolved state, initially prepared as a minimum-uncertainty Gaussian (32) (bold blue circle in panels a,b is its contour enclosing a Planck cell), at time  $t = 20$  in the quartic double well (30) with  $\Delta = 6$  at an energy  $E = -0.958333$  below the barrier top, for the semiclassical approximation (10, 11) (panel b), compared to an exact quantum calculation (37) (a). The initial centroid is  $(q_0, p_0) = (2, 0)$ . Color code as in Fig. 3.

### G. Propagation in the presence of classical chaos

Besides dynamical coherence effects, complex classical dynamics constitutes a major challenge for propagation schemes in molecular physics. The two one-dimensional models discussed in the preceding subsections are strongly anharmonic but remain integrable. In order to test our method also in the presence of chaos and to check its scalability towards higher dimensions, we consider a two-freedom system consisting of Morse oscillators coupled linearly through the positions, a standard model for complex molecular dynamics [90], with a potential

$$V_{2\text{Morse}}(q_1, q_2) = V_{\text{Morse}}(q_1) + V_{\text{Morse}}(q_2) + cq_1q_2, \quad (35)$$

where  $V_{\text{Morse}}(q_i)$ ,  $i = 1, 2$  are Morse potentials (29) and  $c$  is the coupling parameter. Starting from regular dynamics at  $c = 0$ , the system follows the Kolmogorov-Arnol'd-Moser scenario [91] with increasing  $c$  and becomes fully chaotic for  $c \gg 1$ . We here concentrate on the value  $c = 0.3$ , where phase space is mixed. As initial condition, we choose a two-dimensional minimum-uncertainty Gaussian  $W(\mathbf{r}) = W(\mathbf{r}_1)W(\mathbf{r}_2)$ , with  $W(\mathbf{r}_i)$ ,  $i = 1, 2$ , as in Eq. (32), centered within a major chaotic subregion, see inset of Fig. 18.

The autocorrelation function depicted in the main part of Fig. 18 includes the first major revival. The van-Vleck-based Wigner propagator reproduces the exact quantum result reasonably well and shows a tendency to improve on the classical data, evidencing the rôle

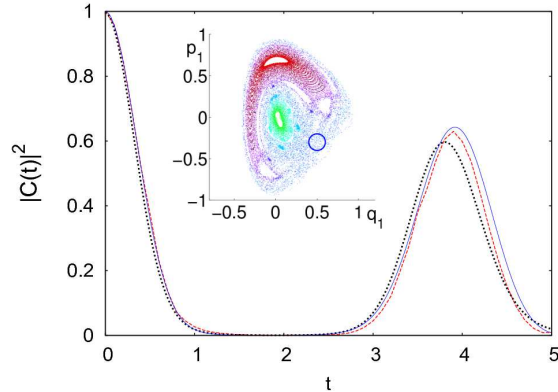


FIG. 18: As Fig. 6 but for two coupled Morse potentials (35) at  $c = 0.3$ . Parameter values are  $m = 1$ ,  $D = 1$ ,  $a = 1.25$ ,  $\hbar = 0.125$ , the initial centroid is  $(q_{10}, p_{10}, q_{20}, p_{20}) = (0.5, -0.3, 0.4322, 0)$ , corresponding to a total energy  $E = 0.5$ . Inset: Poincaré surface of section at  $p_2 = 0$  of the corresponding classical dynamics. Different initial conditions encoded by colors. The blue circle is the contour of the initial Gaussian enclosing a Planck cell.

of dynamical quantum effects in this system.

## IV. ALGORITHMS

In view of the objective to demonstrate the viability of semiclassical Wigner propagation for numerical applications, we indicate in this section how to construct suitable algorithms for this purpose, without entering into details of their implementation.

### A. Assembling the propagator

#### 1. Exact quantum calculation

For purposes of comparison, calibration, etc. it is convenient to have an algorithm available for a direct exact calculation of the quantum propagator, independent of semiclassical approximations. We briefly sketch in the sequel how this is achieved for the propagator of the Wigner function.

Substituting the unitary time-evolution operator  $\hat{U}(t) = \sum_{\alpha} e^{-iE_{\alpha}t/\hbar} |\alpha\rangle\langle\alpha|$  expanded in eigenstates  $|\alpha\rangle$ ,  $\hat{H}|\alpha\rangle = E_{\alpha}|\alpha\rangle$ , in the definition (4), we obtain the Weyl propagator

$U_W(\mathbf{r}, t) = \sum_{\alpha} e^{-iE_{\alpha}t/\hbar} W_{\alpha}(\mathbf{r})$  in terms of Wigner eigenfunctions  $W_{\alpha}(\mathbf{r})$ , Eq. (1) with  $\hat{\rho} = |\alpha\rangle\langle\alpha|$ . By means of the convolution (5), this yields the Wigner propagator in the form

$$G_W(\mathbf{r}'', \mathbf{r}', t) = \sum_{\alpha, \beta} e^{-i(E_{\beta} - E_{\alpha})t/\hbar} \int d^{2f} R e^{\frac{i}{\hbar}(\mathbf{r}'' - \mathbf{r}') \wedge \mathbf{R}} W_{\alpha\alpha} \left( \frac{\mathbf{r}' + \mathbf{r}'' - \mathbf{R}}{2} \right) W_{\beta\beta} \left( \frac{\mathbf{r}' + \mathbf{r}'' + \mathbf{R}}{2} \right). \quad (36)$$

The convolution in Eq. (36) is an inconvenient feature and can be avoided. Combining it with the integrations implicit in the definitions of the Wigner eigenfunctions, it can be evaluated, leading to an expression [92]

$$G_W(\mathbf{r}'', \mathbf{r}', t) = (2\pi\hbar)^f \sum_{\alpha, \beta} e^{\frac{i}{\hbar}(E_{\beta} - E_{\alpha})t} W_{\alpha\beta}^*(\mathbf{r}') W_{\alpha\beta}(\mathbf{r}''), \quad (37)$$

which involves generalized Wigner functions [71]

$$W_{\alpha\beta}(\mathbf{r}) = \frac{1}{2\pi\hbar} \int d^f q' e^{\frac{i}{\hbar} \mathbf{p} \cdot \mathbf{q}'} \left\langle \mathbf{q} + \frac{\mathbf{q}'}{2} \left| \hat{\rho}_{\alpha\beta} \right| \mathbf{q} - \frac{\mathbf{q}'}{2} \right\rangle, \quad (38)$$

with  $\hat{\rho}_{\alpha\beta} = |\alpha\rangle\langle\beta|$ . In the diagonal case  $\alpha = \beta$ , they correspond to the Wigner representation of pure states. For  $\alpha \neq \beta$ , they are not generally real as are the diagonal ones (1) but Hermitian,  $W_{\alpha\beta}(\mathbf{r}) = W_{\beta\alpha}^*(\mathbf{r})$ . Both forms, (36) as well as (37), are consistent with the group properties of the propagator, in particular with the initial condition  $G_W(\mathbf{r}'', \mathbf{r}', 0) = \delta(\mathbf{r}'' - \mathbf{r}')$ . The quantization required to obtain the basis states  $|\alpha\rangle$  can be circumvented by integrating the Schrödinger equation directly (e.g., by split-operator methods) to propagate the density operator or the wavefunction (for pure states) in a suitable representation, followed by a Weyl transform (1).

## 2. Semiclassical approximation based on path integrals

Equations (20, 21) reduce the calculation of the Wigner propagator in the path-integral-based approximations to quadratures. More problematic from a practical point of view is obtaining the necessary input, since it comprises not only second- but even third-order derivatives, see Eq. (21), of the potential—an unavoidable feature, in view of the fundamental rôle the anharmonicity of the potential plays for Wigner propagation.

This disadvantage is compensated for by the fact that this approximation, at least for weak anharmonicity, is accurate enough to allow for a propagation based on a centroid trajectory only, in analogy to Gaussian wavepacket propagation. It then suffices to evaluate

representative values  $\omega$  and  $\sigma$ , respectively, of the second and third derivatives of the potential in the relevant phase-space region, keeping them constant for an entire propagation step, Eqs. (23) or (28), till the next update, e.g., in on-the-fly *ab-initio* molecular dynamics [27, 28].

### 3. *van-Vleck-based semiclassical approximation*

The Eqs. (10, 11) defining the semiclassical Wigner propagator in van Vleck approximation translate into the following straightforward algorithm to compute the propagator as such, not operating on any admissible initial Wigner function:

1. *Initial state:* Define pairs of initial points  $\mathbf{r}'_{j\pm}$ ,  $j = 1, \dots, N$ , with common midpoint  $\mathbf{r}' = (\mathbf{r}'_{j+} + \mathbf{r}'_{j-})/2$ , parameterized, e.g., by spherical coordinates relative to  $\mathbf{r}'$ . A typical value for the number of classical trajectories, used in most of the calculations for one-dimensional systems underlying this paper, is  $N = 10^6$ , corresponding to  $5 \times 10^5$  data points available for the final coarse-graining, step 3b below.
2. *Time steps:* Realize the integration over time as a sequence of  $L$  steps  $t_{l-1} \rightarrow t_l$ ,  $l = 1, \dots, L$ ,  $t_l = t' + l\Delta t$ ,  $\Delta t = (t'' - t')/L$ . Update the basic ingredients of the propagator (10, 11) as follows:

- (a) *Trajectories*  $\mathbf{r}_j(t_l)$ ,  $j = 1, \dots, N$ , according to the classical force field,

$$\Delta \mathbf{r}_j(t_l) = \mathbf{J}^t \nabla H[\mathbf{r}_j(t_l)] \Delta t. \quad (39)$$

- (b) *Stability matrices* according to the evolution equation  $\dot{\mathbf{M}} = \mathbf{M} \mathbf{J}^t \partial^2 H(\mathbf{r}) / \partial \mathbf{r}^2$  (see, e.g., [93]),

$$\Delta \mathbf{M}_j(t_l) = \mathbf{M}_j(t_l) \mathbf{J}^t \frac{\partial^2 H(\mathbf{r}_j(t_l))}{\partial \mathbf{r}_j^2(t_l)} \Delta t. \quad (40)$$

It suggests itself to implement (a) and (b) as a single step, merging Eqs. (39, 40) into a single system of linear equations.

- (c) *Actions*  $S_j$  as (cf. Fig. 1)

$$\Delta S_j(\mathbf{r}'', \mathbf{r}') = [\mathbf{r}_{j+}(t_l) - \mathbf{r}_{j-}(t_l)] \wedge [\Delta \mathbf{r}_{j-}(t_l) + \Delta \mathbf{r}_{j+}(t_l)] / 2 - [H(\mathbf{r}_{j-}(t_l)) - H(\mathbf{r}_{j+}(t_l))] \Delta t.$$

3. *Final state:*

(a) Separate elliptic from hyperbolic trajectory pairs according to

$$\text{traj. pair } j \text{ is } \begin{cases} \text{ell.} & \det [\mathbf{M}_{j_+} - \mathbf{M}_{j_-}] > 0, \\ \text{hyp.} & \det [\mathbf{M}_{j_+} - \mathbf{M}_{j_-}] < 0. \end{cases} \quad (41)$$

- (b) Within each of the two sheets, coarse-grain the determinantal prefactor  $|\det [\mathbf{M}_+(t) - \mathbf{M}_-(t)]|^{-1/2}$  and the action  $S(t)$  by suitable binning with respect to  $\mathbf{r}''$ . In this step, a possibly inhomogeneous distribution of the initial points (as, e.g., for polar coordinates) must be accounted for in terms of weight factors.
- (c) Calculate the propagator (10) for each sheet and superpose the two contributions.

## B. Propagating smooth localized initial states: towards Monte Carlo algorithms

For the more common task of propagating well-localized but quantum-mechanically admissible initial states (e.g., Gaussians), the method described in the previous subsection is not optimal. We can take advantage of the fact that a common midpoint of all trajectory pairs is not specified, by evaluating all the  $N(N-1)/2$  pairs formed by a set of  $N$  classical trajectories to gain a factor  $O(N)$  in efficiency. We have to take into account, however, that the distribution of centers  $\bar{\mathbf{r}}_{jk} = (\mathbf{r}_j + \mathbf{r}_k)/2$  of an ensemble of “satellite” phase-space points  $\mathbf{r}_j$ , distributed at random or on an ordered grid with probability density  $p_{\text{sat}}(\mathbf{r})$ , is not this density but its self-convolution,  $p_{\text{ctr}}(\bar{\mathbf{r}}) = \int d^{2f}r p_{\text{sat}}(\bar{\mathbf{r}} - \mathbf{r}/2)p_{\text{sat}}(\bar{\mathbf{r}} + \mathbf{r}/2)$ . For Gaussians (31) this reduces to a contraction by a factor  $\sqrt{2}$ .

Accordingly, we propose the following scheme for the propagation of smooth localized initial states:

1. *Initial state:* Define a set of initial points  $\mathbf{r}'_j$ ,  $j = 1, \dots, N_{\text{sat}}$ . A typical value  $N_{\text{sat}} = 1000$  now generates  $N_{\text{ctr}} = 5 \times 10^5$  final data points. This can be done in two ways:
  - (a) Generate a swarm of random phase-space points  $\mathbf{r}'_j$  covering approximately the same phase-space region as the intended initial Wigner function  $W_{\text{ctr}}(\mathbf{r}')$ , and associate the weight  $W_{\text{ctr}}(\bar{\mathbf{r}}'_{jk}, t')$  to each pair with midpoint  $\bar{\mathbf{r}}'_{jk}$ ,  $j = 1, \dots, N_{\text{sat}}$ ,  $k = 1, \dots, j - 1$ .

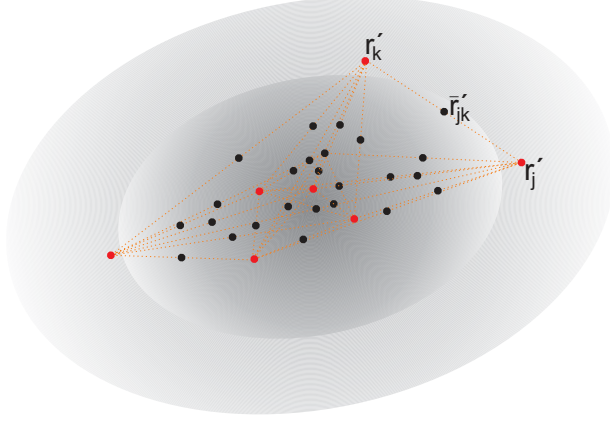


FIG. 19: Preparation of initial points for the propagation algorithm for smooth initial distributions, Subsection IV B. An ensemble of random “satellite” points  $\mathbf{r}'_j$ ,  $j = 1, \dots, N_{\text{sat}}$  (red dots) which serve as initial points of  $N_{\text{sat}}$  classical trajectories give rise to  $N_{\text{ctr}} = N_{\text{sat}}(N_{\text{sat}} - 1)/2$  midpoint paths  $\bar{\mathbf{r}}_{jk}(t)$  starting in the centers  $\bar{\mathbf{r}}'_{jk} = (\mathbf{r}'_j + \mathbf{r}'_k)/2$  (black dots) and define the support of the propagator at the final time  $t$ . The distribution  $p_{\text{ctr}}(\bar{\mathbf{r}}'_{jk})$  (dark grey) of the centers is that of the satellites  $p_{\text{sat}}(\mathbf{r}'_j)$  (light) contracted by a factor  $\sqrt{2}$ .

- (b) (For Gaussian initial states only) Find the distribution  $W_{\text{sat}}(\mathbf{r}', t')$  with covariance matrix  $\mathbf{A}_{\text{sat}} = \mathbf{A}_{\text{ctr}}/\sqrt{2}$  that entails the intended  $W_{\text{ctr}}(\bar{\mathbf{r}}'_{jk}, t')$  as its center distribution and generate the  $\mathbf{r}'_j$  according to  $W_{\text{sat}}(\mathbf{r}', t')$  (Fig. 19).
2. *Time steps:* Propagate classically all  $N_{\text{sat}}$  satellites  $\mathbf{r}'_j$  as described in step 2 above.
3. *Final state:* Proceed as in step 3 above for every final midpoint  $\bar{\mathbf{r}}''_{jk}$ . If option 1b above has been chosen, assign the corresponding weights  $W_{\text{ctr}}(\bar{\mathbf{r}}'_{jk}, t')$  to the midpoints  $\bar{\mathbf{r}}''_{jk}$  in the final coarse-graining.

Being based on ensembles of random phase-space points distributed according to some initial density, this propagation scheme readily integrates in Metropolis-type algorithms. This suggests itself particularly in the case of high-dimensional spaces where a direct evaluation of the phase-space integrals involved would be prohibitive.

## V. CONCLUSION

The present work is intended to trigger an interdisciplinary “technology transfer”, promoting the application in molecular physics of a semiclassical phase-space propagation scheme that emerged in quantum chaos. We offer a detailed survey of semiclassical Wigner propagation, focussing on its implementation and performance as a numerical tool that provides a natural initial-value representation. Two complementary approaches to semiclassical approximations of the Wigner propagator are considered, one based on the van-Vleck propagator, including nondiagonal contributions to orbit sums, the other on phase-space path integration combined with an expansion of the phase. The former possesses a clear-cut classical skeleton in terms of symplectic geometry, is surprisingly accurate in significantly nonlinear systems—more so in the reproduction of the notorious fine nodeline structure of the Wigner function than in absolute values—and easily generalizes to high-dimensional phase spaces. Two known evils of semiclassical propagation, however, return through the back door: caustics, now in phase space, and loss of normalization.

The path-integral approach, by contrast, provides a very precise description at weak yet finite anharmonicity. It resolves caustics in terms of Airy functions but tends to fail at strong nonlinearity and does not readily extend to higher dimensions. In addition, we devise a hybrid based on the same robust structure of trajectory pairs as the van Vleck approach but augmented by a uniform approximation to improve the accuracy in the case of close stationary points. It appears particularly suitable for heavy-duty numerical applications, as in *ab-initio* molecular-dynamics simulations [27, 28] where integration times between updates of the potential are relatively short but the number of freedoms is large and access to second- and higher-order derivatives of the potential is exceedingly costly.

In view of the relatively little that is known to date about semiclassical Wigner propagation, our results provide sufficient qualitative and quantitative evidence to invalidate two popular connotations: The approach readily captures the time evolution of quantum coherence effects, including specifically the propagation of Schrödinger-cat states and the reproduction of tunneling processes. In these cases, it is crucial that even trajectory pairs with large initial separation be taken into account. At the same time, we found that the notion of propagating along any kind of “quantum trajectory” is lacking support. While the deterministic delta function on the classical trajectory that constitutes the Liouville prop-

agator is replaced by a smooth quantum spot, no enhancement of this spot on any other deterministic propagation path is observed.

Various open ends of this work remain to be explored, of which we mention but a few:

- i. Extending semiclassical Wigner propagation to higher dimensions. It is significantly facilitated by the transparent geometric underpinning and by viable options to adapt it to Monte-Carlo algorithms.
- ii. Semiclassical Wigner propagation in mixed and even fully chaotic systems. Recent work in the context of quantum chaos [58] suggests it should work well, but it awaits being tested in molecular-physics applications.
- iii. Complexifying phase space. A promising option how to improve on our trajectory-based semiclassical approximations, it would resolve caustics and enable a comprehensive description of tunneling.
- iv. Including incoherent processes like dephasing and dissipation, possibly at finite temperature. While this requires major modifications of semiclassical approximations made for pure states [94], semiclassical Wigner propagation along trajectory pairs readily extends to systems with Markovian dissipation [31]. Alternatively, the Feynman-Vernon influence-functional theory [95, 96] combines well with phase-space path integration to achieve high-accuracy semiclassical propagation even in the presence of memory effects [97].

### **Acknowledgements**

We enjoyed inspiring discussions with Marcus de Aguiar, Frank Großmann, Gert In-gold, Jürgen Korsch, Dominik Marx, Alfredo Ozorio, Eli Pollak, Uzy Smilansky, and Carlos Viviescas. Financial aid from Volkswagen Foundation (grant I/78 235, for TD and EAG), Colciencias (for LAP), Universidad Nacional de Colombia, and the ALECOL program of the German Academic Exchange Service DAAD (for EAG) is gratefully acknowledged. We thank for the hospitality extended to us by the Brazilian Center for Physics Research CBPF, Rio de Janeiro, MPI for the Physics of Complex Systems, Dresden, University of Technology



Kaiserslautern, and University of Augsburg, where parts of this work were carried out.

---

- [1] E. Runge and E. K. U. Gross. *Phys. Rev. Lett.*, 52:997, 1984.
- [2] R. B. Gerber, V. Buch, and M. A. Ratner. *J. Chem. Phys.*, 77:3022, 1982.
- [3] H. D. Meyer, U. Manthe, and L. S. Cederbaum. *Chem. Phys. Lett.*, 165:73, 1990.
- [4] M. A. Sepúlveda and F. Grossmann. *Adv. Chem. Phys.*, 96:191, 1996.
- [5] M. V. Berry and K. E. Mount. *Rep. Prog. Phys.*, 35:315, 1972.
- [6] J. H. van Vleck. *Proc. Natl. Acad. Sci. USA*, 14:178, 1928.
- [7] M. C. Gutzwiller. *J. Math. Phys.*, 8:1979, 1967.
- [8] R. G. Littlejohn. *J. Stat. Phys.*, 68:7, 1992.
- [9] W. H. Miller. *Adv. Chem. Phys.*, 25:69, 1974.
- [10] S. Levit and U. Smilansky. *Ann. Phys. (N. Y.)*, 108:165, 1977.
- [11] S. Levit, K. Möhring, U. Smilansky, and T. Dreyfus. *Ann. Phys. (N. Y.)*, 114:223, 1978.
- [12] J. R. Klauder. *Phys. Rev. Lett.*, 56:897, 1986.
- [13] W. H. Miller. *Faraday Discuss.*, 110:1, 1998.
- [14] M. Thoss, H. Wang, and W. H. Miller. *J. Chem. Phys.*, 114:9220, 2001.
- [15] J. Liu and W. H. Miller. *J. Chem. Phys.*, 125:224104, 2006.
- [16] W. H. Miller. *J. Phys. Chem. A*, 105:2942, 2001.
- [17] M. Thoss and H. Wang. *Annu. Rev. Phys. Chem.*, 55:299, 2004.
- [18] K. G. Kay. *Annu. Rev. Phys. Chem.*, 56:255, 2005.
- [19] E. J. Heller. *J. Chem. Phys.*, 62:1544, 1975.
- [20] M. F. Herman and E. Kluk. *Chem. Phys.*, 91:27, 1984.
- [21] F. Grossmann. *Comments At. Mol. Phys.*, 34:141, 1999.
- [22] M. Baranger, M. A. M. de Aguiar, F. Keck, H. J. Korsch, and B. Schellhaaß. *J. Phys. A: Math. Gen.*, 34:7227, 2001.
- [23] E. J. Heller. *J. Chem. Phys.*, 94:2723, 1991.
- [24] J. Vaníček. *Phys. Rev. E*, 70:055201(R), 2004.
- [25] J. Vaníček. *Phys. Rev. E*, 73:046204, 2006.
- [26] B. Li, C. Mollica, and J. Vaníček. *J. Chem. Phys.*, 131:041101, 2009.
- [27] D. Marx, M. E. Tuckerman, and G. J. Martyna. *Comput. Phys. Commun.*, 118:166, 1999.

- [28] N. L. Doltsinis and D. Marx. *J. Theor. Comp. Chem.*, 1:319, 2002.
- [29] M. Ceotto, S. Atahan, and A. Aspuru-Guzik. *arXiv 0424.0712 [cond.mat.mtrl-sci]*, 2007.
- [30] J. Tatchen and E. Pollak. *J. Chem. Phys.*, 130:041103, 2009.
- [31] A. M. Ozorio de Almeida, P. de M. Rios, and O. Brodier. *J. Phys. A: Math. Theor.*, 42:065306, 2009.
- [32] K. Husimi. *Proc. Phys. Math. Soc. Japan*, 22:264, 1940.
- [33] J. R. Klauder and B. S. Skagerstam. *Coherent States: Applications in Physics and Mathematical Physics*. World Scientific, Singapore, 1985.
- [34] J. R. Klauder. *Phys. Rev. D*, 19:2349, 1979.
- [35] E. P. Wigner. *Phys. Rev.*, 40:749, 1932.
- [36] M. Hillery, R. F. O’Connell, M. O. Scully, and E. P. Wigner. *Phys. Rep.*, 106:121, 1984.
- [37] W. P. Schleich. *Quantum Optics in Phase Space*. Wiley–VCH, Berlin, 2001.
- [38] M. V. Berry. *Phil. Trans. Roy. Soc. (London) A*, 287:237, 1977.
- [39] W. H. Zurek. *Nature*, 412:712, 2001.
- [40] E. J. Heller. *J. Chem. Phys.*, 65:1289, 1976.
- [41] F. McLafferty. *J. Chem. Phys.*, 78:3253, 1983.
- [42] M. Grønager and N. E. Henriksen. *J. Chem. Phys.*, 100:5387, 1995.
- [43] H. W. Lee and M. O. Scully. *J. Chem. Phys.*, 77:4604, 1982.
- [44] H. W. Lee. *J. Found. Phys.*, 22:995, 1992.
- [45] M. Razavy. *Phys. Lett. A.*, 119:212, 1996.
- [46] A. Donoso and C. C. Martens. *Phys. Rev. Lett.*, 87:223202, 2001.
- [47] C. J. Trahan, K. Hughes, and R. E. Wyatt. *J. Chem. Phys.*, 118:9911, 2003.
- [48] J. Moix, E. Pollak, and J. Shao. *Phys. Rev. A*, 80:052103, 2009.
- [49] M. S. Marinov and B. Segev. *Phys. Rev. A*, 54:4752, 1996.
- [50] E. J. Heller. *J. Chem. Phys.*, 67:3339, 1977.
- [51] A. M. Ozorio de Almeida. *Phys. Rep.*, 295:265, 1998.
- [52] M. V. Berry. *Proc. Roy. Soc. Lond. A*, 423:219, 1989.
- [53] O. Agam and S. Fishman. *Phys. Rev. Lett.*, 73:806, 1998.
- [54] F. Toscano, M. A. M. de Aguiar, and A. M. Ozorio de Almeida. *Phys. Rev. Lett.*, 86:59, 2001.
- [55] P. P. de M. Rios and A. M. Ozorio de Almeida. *J. Phys. A: Math. Gen.*, 35:2609, 2002.
- [56] T. Dittrich, C. Viviescas, and L. Sandoval. *Phys. Rev. Lett.*, 96:070403, 2006.

- [57] M. S. Marinov. *Phys. Lett. A*, 153:5, 1991.
- [58] T. Dittrich and L. A. Pachón. *Phys. Rev. Lett.*, 102:150401, 2009.
- [59] D. Galetti and A. F. R. de Toledo Piza. *Physica*, 149A:267, 1988.
- [60] N. L. Balazs. *Physica*, 102A:236, 1980.
- [61] R. P. Feynman. *Rev. Mod. Phys.*, 20:367, 1948.
- [62] L. S. Schulman. *Techniques and Applications of Path Integration*. Wiley, New York, 1981.
- [63] If the propagator in original phase space takes the form  $G_W(\boldsymbol{\rho}'', \boldsymbol{\rho}', t) = g(\boldsymbol{\rho}'' - \mathbf{M}(t)\boldsymbol{\rho}')$ , with  $g(\boldsymbol{\rho})$  some normalizable distribution and  $\mathbf{M}(t)$  a symplectic matrix generating a linearized canonical transformation, then the Fourier-transformed propagator can be written as  $\tilde{G}_W(\boldsymbol{\gamma}'', t; \boldsymbol{\gamma}', 0) = (2\pi)^{-1} \tilde{g}(\boldsymbol{\gamma}'') \delta(\boldsymbol{\gamma}'' - \mathbf{M}(t)\boldsymbol{\gamma}')$ , where  $\tilde{g}(\boldsymbol{\gamma})$  is the Fourier transform of  $g(\boldsymbol{\rho})$ . This reduces the equivalent of Eqs. (2,3) in Fourier space to multiplications.
- [64] M. Abramowitz and I. A. Stegun (eds.). *Pocketbook of Mathematical Functions*. Harri Deutsch, Thun, 1984.
- [65] O. Vallée and M. Soares. *Airy Functions and Applications to Physics*. Imperial College Press, London, 2004.
- [66] R. Carles, C. Fermanian-Kammerer, N. J. Mauser, and H. P. Stimming. *Commun. Pure Appl. Anal.*, 8:559, 2009.
- [67] H. Kobeissi and M. Korek. *Int. J. Quant. Chem.*, 39:23, 2004.
- [68] O. Bayrak and I. Boztosun. *J. Phys. A: Math. Gen.*, 39:6955, 2006.
- [69] C. E Burkhardt and J. J. Leventhal. *Am. J. Phys.*, 75:686, 2007.
- [70] U. Roy and S. Ghosh. *arXiv:0907.3116v1 [quant-ph]*, 2009.
- [71] J. P. Dahl and M. Springborg. *J. Chem. Phys.*, 88:4535, 1988.
- [72] C. Harabati, J. M. Rost, and F. Grossmann. *J. Chem. Phys.*, 120:26, 2004.
- [73] A. Kenfack, J. M. Rost, and A. M. Ozorio de Almeida. *J. Phys. B: At. Mol. Opt. Phys.*, 37:1645, 2004.
- [74] P. M. Morse. *Phys. Rev.*, 34:57, 1929.
- [75] M. Hug, C. Menke, and W. P. Schleich. *J. Phys. A: Math. Gen.*, 31:L217, 1998.
- [76] M. Hug, C. Menke, and W. P. Schleich. *Phys. Rev. A.*, 57:3188; *ibid.* 3206, 1998.
- [77] A. Frank, A. L. Rivera, and K. B. Wolf. *Phys. Rev. A.*, 61:054102, 2000.
- [78] J. Stanek and J. Konarski. *Int. J. Quant. Chem.*, 103:10, 2006.
- [79] D. T. Smithey, M. Beck, M. G. Raymer, and A. Faridani. *Phys. Rev. Lett.*, 70:1244, 1993.

- [80] R. L. Hudson. *Rep. Math. Phys.*, 6:249, 1974.
- [81] E. J. Heller. Wavepacket dynamics and quantum chaology. In M.-J. Giannoni, A. Voros, and J. Zinn-Justin, editors, *Chaos and Quantum Physics*, volume LII of *Les Houches Lectures*, page 547. North-Holland, Amsterdam, 1991.
- [82] K. G. Kay. *J. Chem. Phys.*, 100:4432, 1994.
- [83] L. M. K. Vandersypen, M. Steffen, G. Breyta, C. S. Yannon, M. H. Sherwood, and I. L. Chuang. *Nature*, 414:883, 2001.
- [84] L. D. Landau and I. M. Lifshitz. *Quantum Mechanics (Nonrelativistic Theory)*. Pergamon, Oxford, 1965.
- [85] S. C. Creagh. *J. Phys. A: Math. Gen.*, 27:4969, 1994.
- [86] A. L. Xavier Jr. and M. A. M. de Aguiar. *Phys. Rev. Lett*, 79:3323, 1997.
- [87] N. L. Balazs and A. Voros. *Ann. Phys. (N. Y.)*, 199:123, 1990.
- [88] M. Novaes. *J. Math. Phys.*, 46:102102, 2005.
- [89] M. S. Marinov and B. Segev. *Phys. Rev. A*, 55:3580, 1997.
- [90] C. Jung, E. Ziemniak, M. Carvajal, A. Frank, and R. Lemus. *Chaos*, 11:464, 2001.
- [91] A. J. Lichtenberg and M. A. Lieberman. *Regular and Chaotic Dynamics*. Number 38 in Applied Mathematical Sciences. Springer, New York, 2nd edition, 1992.
- [92] A. Argüelles and T. Dittrich. *Physica A*, 356:72, 2005.
- [93] F. Grossmann. *J. Chem. Phys.*, 125:014111, 2006.
- [94] C.-M. Goletz and F. Grossmann. *J. Chem. Phys.*, 130:244107, 2009.
- [95] R. P. Feynman and F. L. Vernon, Jr. *Ann. Phys. (N. Y.)*, 24:118, 1963.
- [96] A. O. Caldeira and A. J. Leggett. *Physica*, 121A:587, 1983.
- [97] H. Grabert, P. Schramm, and G.-L. Ingold. *Phys. Rep.*, 168:115, 1988.